Generation and characterization of a murine model for Hereditary Spastic Paraplegia SPG11

Dissertation
zur Erlangung des akademischen Grades
doctor rerum naturalium (Dr. rer. nat.)

vorgelegt dem Rat der Medizinischen Fakultät
der Friedrich-Schiller-Universität Jena

von Rita Eva Varga (MSc)
geboren am 25.08.1984 in Debrecen, Ungarn

Gutachter:

1. Prof. Dr. Christian Hübner
   Institute of Human Genetics, University Hospital Jena, Germany
2. Prof. Dr. Christoph Biskup
   Biomolecular Photonics Group, University Hospital Jena, Germany
3. Prof. Dr. Thomas Braulke
   Department of Biochemistry, Children's Hospital, University Medical Center Hamburg-Eppendorf

Tag der öffentlichen Verteidigung: 02.02.2016

List of abbreviations

AD	Autosomal dominant
AF	Autofluorescence
ALS	Amyotrophic lateral sclerosis
ALR	Autophagic lysosome reformation
ANOVA	Analysis of variance
AP	Adaptor protein
AR	Autosomal recessive
βgeo	β-galactosidase/neomycin
$CaCl_2$	Calcium chloride
Calb	Calbindin
cDNA	Complementary deoxyribonucleic acid
CH_3COOH	Acetic acid
CNS	Central nervous system
cpm	Counts per minute
CsCl	Caesium chloride
Ctx	Cortex
CtsDp	Cathepsin D precursor
CtsDm	Cathepsin D mature
dATP	Deoxyadenosin triphosphate
dCTP	Deoxycytidin triphosphate

dGTP	Deoxyguansin triphosphate
DMSO	Dimethyl sulfoxide
DNA	Deoxyribonucleic acid
dTTP	Deoxythymidin triphosphate
EDTA	Ethylenediaminetetraacetic acid
ES cells	Embryonic stem cells
EtOH	Ethanol
GAPDH	Glyceraldehyde phosphate dehydrogenase
GFAP	Glial fibrillary acidic protein
GFP	Green fusion protein
GL	Granular layer
H_2O	Water
HCl	Hydrochloric acid
HBSS	Hank's balanced salt solution
HEPES	4-(2-hydroxyethyl)-1-piperazineethanesulfonic acid
HRP	Horseradish peroxidase
HSP	Hereditary spastic paraplegia
K^+	Potassium
kb	Kilobase
KCl	Potassium chloride
kDa	Kilodalton
KH_2PO4	Potassium dihydrogen phosphate

KIF	Kinesin family member
KO	Knockout
Lamp1	Lysosomal-associated membrane protein 1
LB	Lysogeny broth
LC3	Microtubule-associated protein 1 light chain 3
LiCl	Lithium chloride
LMP	Lysosomal membrane proteins
$MgCl_2$	Magnesium chloride
M	Mole
m	Milli
mm	Millimeter
MEF	Mouse embryonic fibroblast
$MgSO_4$	Magnesium sulfate
ML	Molecular layer
MOPS	3-(N-morpholino)propanesulfonic acid
M6PR	Mannose-6-phosphate receptor
mRNA	Messenger ribonucleic acid
n	Number
nM	Nanomole
Na^+	Sodium
NaCl	Sodium chloride
NaF	Sodium Fluoride

Na_2HPO_4	Disodium hydrogen phosphate
NaOH	Sodium Hydroxide
NCL	Neuronal ceroid lipofuscinosis
NH_4Cl	Ammoniumchloride
NPC	Niemann-Pick disease, type C
OD	Optical density
pA	Polyadenylation site
PBS	Phosphate-buffered saline
PC	Purkinje cell
PCR	Polymerase chain reaction
PEG	Polyethylene glycol
PFA	Paraformaldehyde
PKC	Protein kinase C
PNS	Peripheral nervous system
RbCl	Rubidium chloride
RNA	Ribonucleic acid
RNase	Ribonuclease
RPM	Revolutions per minute
RT	Room temperature
SA	Splice acceptor site
SDS	Sodium dodecyl sulfate
SEM	Standard error of the mean

SOC	Super optimal broth with catabolite repression
SPG	Spastic gait locus
SSC	Saline sodium citrate
SSPE	Saline sodium citrate phosphate EDTA
TAE	Tris-acetate-EDTA
TGN	Trans-Golgi-network
TBST	Tris-buffered saline added with Tween 20
TE	Tris-EDTA
Tris	Tris(hydroxymethyl)aminomethane
U	Unit
UV	Ultraviolet
V	Voltage
α	Alpha
β	Beta
μ	Mikro
ζ	Zeta
ψ	Psi

Table of contents

Summary

Hereditary spastic paraplegias (HSPs) are clinically and genetically heterogenous group of movement disorders characterised mainly by a progressive spastic gait disorder and weakness of the legs, which results from a length-dependent axonopathy of corticospinal tract fibres. HSP type SPG11 is the most common recessive form and is caused by mutations in the *SPG11* gene, which encodes the protein SPATACSIN. The pathophysiology of SPG11 is so far not well understood. In order to study the function of Spatacsin and to elucidate the key events leading to SPG11, *Spg11* was disrupted in mice. Lack of Spatacsin in mice indeed causes a progressive gait disorder, which is paralleled by a progressive loss of cortical neurons and Purkinje cells. Degenerating neurons accumulate autofluorescent material. These deposits are associated with the lysosomal protein Lamp1, p62, a receptor for cargo destined to be degraded by autophagy, and with LC3, a marker for autophagosomes, suggesting that the deposits are related to autolysosomes. Distinct lysosomal functions, such as the processing of Cathepsin D and lysosomal pH do not differ between genotypes. Moreover, the levels of Lamp1 both in brain tissue and mouse embryonic fibroblast (MEF) lysates are not altered in knockout mice. Further supporting a defect in autophagic clearance, in knockout MEFs lipidated LC3 levels are increased and p62 levels are elevated in brain lysates. Consistently, the number of autolysosomes is increased while the number of lysosomes is decreased in KO MEFs. Upon starvation, the number of lysosomes decrease, but the lysosome number recovers upon sustained starvation only in wild-tpye MEFs. A depletion of lysosomes was also evident *in vivo* in Purkinje cells of 2 and 11-month-old knockout mice. These data suggest that owing to the decreased number of lysosomes, available for fusion with autophagosomes in knockout mice, autolysosomal clearance may be impaired which results in the accumulation of un-degraded material and finally causes death of particularly sensitive neurons like cortical motoneurons and Purkinje cells.

Zusammenfassung

Bei hereditären spastischen Paraplegien (HSP) handelt es sich um eine genetisch heterogene Gruppe von Bewegungsstörungen, die hauptsächlich durch einen progressiven spastischen Gang und eine Schwäche der Beine charakterisiert sind. Die Ursache der Erkrankung liegt in einer längenabhängigen Degeneration kortikospinaler Fasern. Die häufigste rezessive Form ist SPG11, welche durch Mutationen des *SPG11*-Gens verursacht wird. *SPG11* kodiert für das Protein SPATACSIN. Bislang ist die Funktion von SPATACSIN weitgehend unverstanden. Um die Funktion von SPATACSIN aufzuklären und die Pathophysiologie der *SPG11*-assoziierten Erkrankung zu verstehen, wurde im Rahmen der vorliegenden Arbeit das *Spg11-Gen* gezielt in Mäusen ausgeschaltet. Der Verlust von Spatacsin führt bei den Knockoutmäusen zu einer progressiven Bewegungsstörung, die mit einem fortschreitenden Verlust kortikaler Neurone und Purkinje Zellen des Kleinhirns einhergeht. In den entsprechenden Neuronenpopulationen kommt es zu einer Akkumulation von autofluoreszierendem Material, das mit dem lysosomalen Protein Lamp1 sowie den Autophagiemarkern p62 und LC3 kolokalisiert. Dies deutet darauf hin, dass das autofluoreszierende Material mit autolysosomalen Strukturen assoziiert ist. Es findet sich keine Hinweise auf eine lysosomale Funktionsstörung der Mäuse im Sinne einer gestörten Cathepsin-D Prozessierung oder einem veränderten lysosomalen pH. Zudem ist weder die Expression von Lamp1 im Gehirn der Knockoutmäuse noch in embryonalen Fibroblasten (MEFs) verändert. Die Untersuchungen weisen vielmehr auf eine gestörte Clearance von Autophagosomen hin. So zeigen sich in MEFs der Knockoutmäuse erhöhte Spiegel von lipid-assoziiertem LC3 sowie ein Anstieg von p62 in Gehirnlysaten. Im Einklang mit dem gestörten Umsatz von Autolysosomen ist deren Anzahl in MEFs von KO-Mäusen erhöht, wohingegen die Anzahl von Lysosomen erniedrigt ist. Nach Hungern der Zellen beider Genotypen kommt es zunächst zu einer erniedrigten Anzahl von Lysosomen, die sich im Verlauf jedoch lediglich in den Wiltypzellen normalisiert.
Die erniedrigte Zahl von Lysosomen kann auch *in vivo* in Purkinje-Zellen von 2 bzw. 11 Monate alten KO Mäusen nachgewiesen werden. Diese Daten zeigen, dass aufgrund der erniedrigten Anzahl von Lysosomen im KO, die für die Fusion mit Autophagosomen zur Verfügung stehen, der autolysosomale Abbau beeinträchtigt

ist. Dies resultiert möglicherweise in der Akkumulation von nicht-degradiertem intrazellulärem Material und mündet im Zelluntergang besonders anfälliger Nervenzellen wie kortikalen Motoneuronen und Purkinje- Zellen.

Introduction

Hereditary spastic paraplegia

Hereditary spastic paraplegias (HSPs) are a heterogeneous group of neurodegenerative movement disorders characterized by a length-dependent distal axonopathy of fibres of the corticospinal tract, which causes lower limb spasticity and weakness (Blackstone et al., 2011; Harding et al., 1983; DeLuca et al., 2004).

The corticospinal tract pathway originates from the layer V of the cerebral motorcortex where the giant long projection pyramidal cells (Betz cells) are located. The axons of these upper motor neurons pass different brain stuctures in order to directly or indirectly (through spinal interneurons) connect with lower motor neurons. Axons of lower motor neurons innervate skeletal muscle (Fig. 1) (Carpenter et al., 1991).

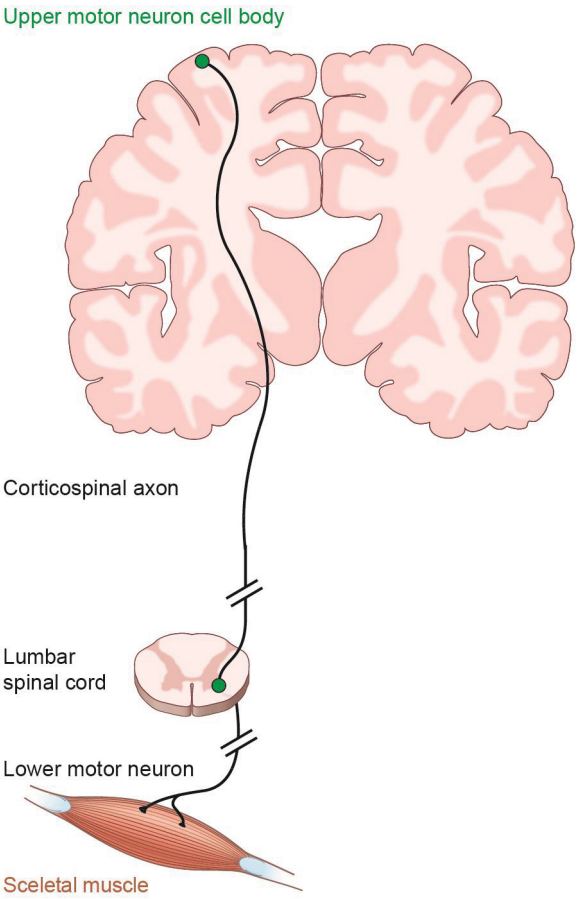

Figure 1. The human corticospinal tract (modified after Blackstone et al., 2011.).

Other CNS structures contribute to motor control, i.e.: basal ganglia, thalamus, midbrain and cerebellum. The latter one helps to maintain balance, adjusts smooth and accurate movements and helps to reduce movement errors. The cerebellar cortex is divided into three layers: the molecular layer, the Purkinje cell layer and the granule layer (Fig. 2). Purkinje cells functionally represent the efferent pathway of the cerebellum. They are arranged in a monolayer (Purkinje cell layer) and have elaborate dendritic fibers that extend to the molecular layer. Interestingly, blockage in the flow of information in the cerebellum leads to cerebellar damage and uncoordinated movement called ataxia (Schmahmann et al., 2004).

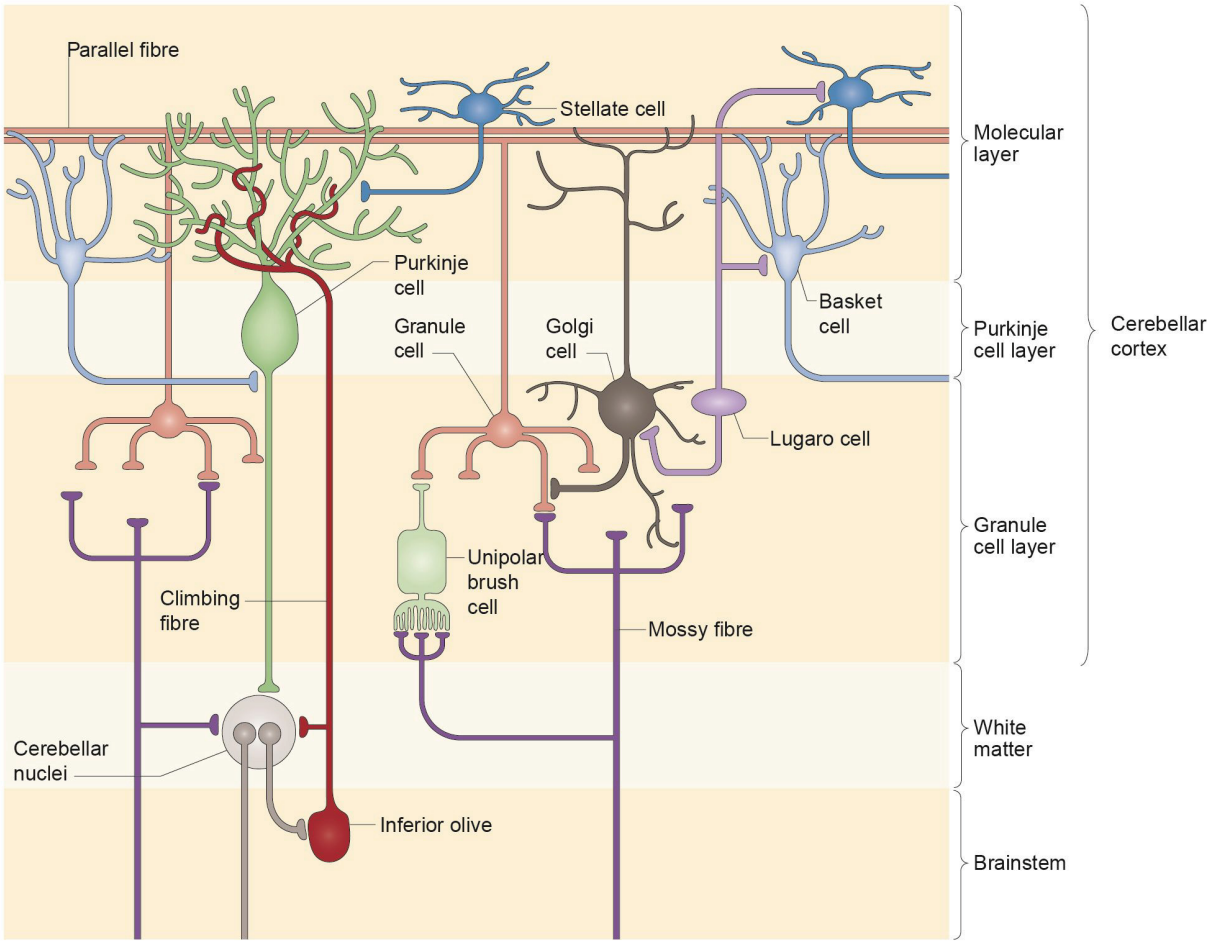

Figure 2. Cerebellar cytoarchitechture (Cerminara et al., 2015).

The axons of cortical motoneurons are extremely long and may reach up to 1 m in length in humans. Because of the long distance between the soma and distal parts of the axon, the life-long maintenance of these axonal structures imposes a considerable challenge for the neuron.

HSP patients typically show an abnormal i.e. ‘spastic’ gait. Because of the time-dependent deterioration of symptoms patients often become wheelchair bound during the course of the disease. Clinically two groups of HSPs are distinguished: the spasticity of legs without additional symptoms defines ‘pure’ forms, whereas the presence of extra clinical features like ataxia, mental retardation, amyotrophy, peripheral neuropathy is observed in ‘clinically complex’ HSP. Age at onset and speed of progression are highly variable both between and within families (Harding et al., 1983; Reid et al., 1999; Depienne et al., 2007). The prevalence of HSP has been estimated as 1-10 in 100.000 (Braschinsky et al., 2008).

HSPs can be inherited as an autosomal dominant (AD), autosomal recessive (AR), or X-linked trait. The most frequent autosomal dominant HSP types are SPG4, SPG3A and SPG31 (Sauter et al., 2002; Faber et al., 2014). SPG11 and SPG15 represent the most common recessive forms (Stevanin et al., 2007; Hanein et al., 2008). SPG1 and SPG2 belong to the X-linked group of HSPs. To date, more than 70 spastic paraplegia gene loci (SPGs) have been identified (Blackstone et al., 2011, Finsterer et al., 2012, Novarino et al., 2014). Thus HSP is highly heterogeneous not only clinically but also genetically.

Proteins encoded by HSP genes fall into different functional categories (Blackstone et al., 2011 and 2012): HSP proteins are thought to play a role in cellular trafficking or shaping of membranes, are involved in the quality control of mitochondrial proteins, mediate axonal outgrowth, myelination and maintain connections between astrocytes and oligodendrocytes, and also affect lipid synthesis and metabolism (Fig. 3).

Currently, no causative therapy is available for HSP. The symptomatic therapy is limited to the reduction of muscle tone and to physiotherapy (Fink et al., 2006). Of note, a murine HSP model has already been successfully treated by gene therapy (Pirozzi et al., 2006). Yet, clarifying the cellular and subcellular pathomechanisms underlying HSP may lead to the development of drugs targeting the cause of the disease (Zuchner et al., 2007), and this knowledge may also be of broader

importance in understanding related neurodegenerative disorders (e.g. lysosomal storage disorders) as well.

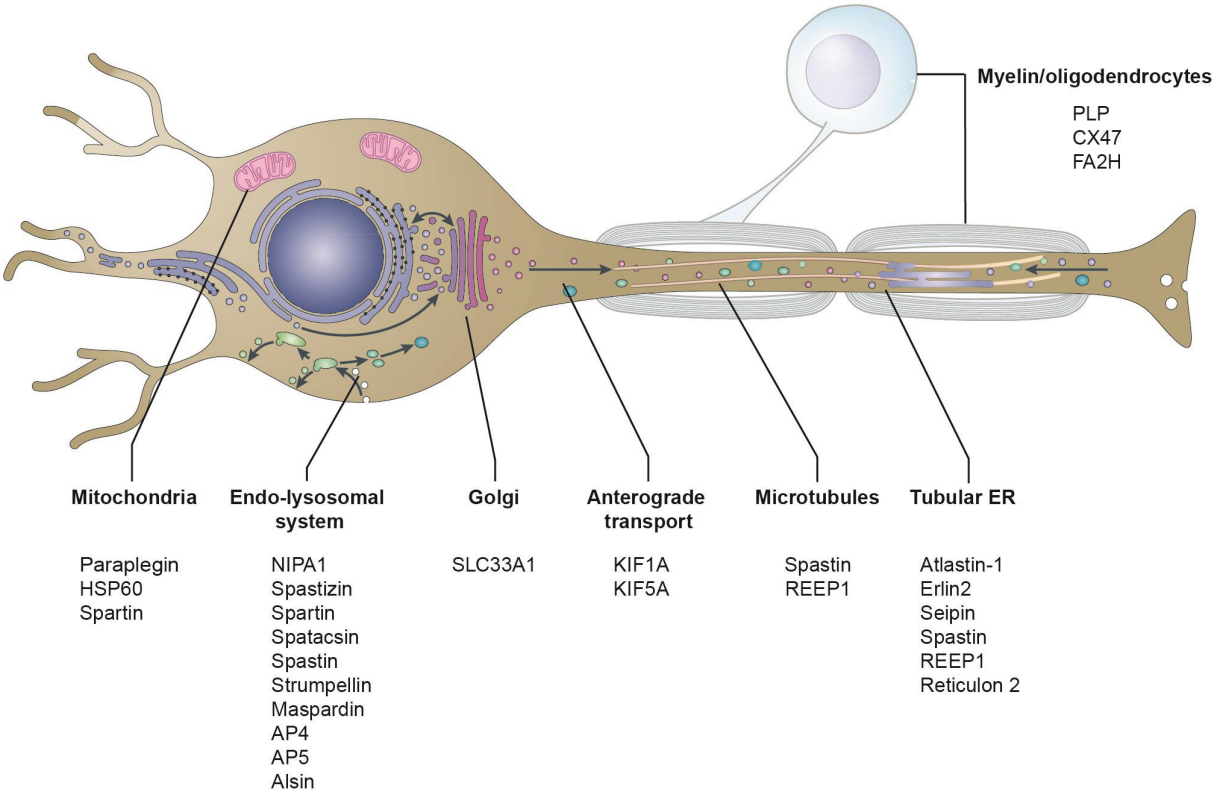

Figure 3. The proposed function of HSP proteins in corticospinal motor neurons (modified from Blackstone et al., 2011 and 2012.).

Hereditary Spastic Paraplegia type 11 (SPG11)

HSP type SPG11 represents the most frequent type of autosomal recessive complex HSPs. Missense, nonsense, and splice site mutations as well as small and gross deletions/ insertions have been detected in SPG11 patients, which are distributed over the entire coding sequence of the gene and most likely confer loss of function of the protein SPATACSIN (Stevanin et al., 2007; Hehr et al., 2007). SPG11 patients not only suffer from spasticity of legs but frequently also from mental retardation, thinning of the corpus callosum, cerebellar defects, and, less commonly, epilepsy, parkinsonism, retinal degeneration, and lower motoneuron damage (Stevanin et al., 2007; Orlén et al., 2009; Anheim et al., 2009; Orlacchio et al., 2010; Pensato et al., 2014).

SPATACSIN represents a large protein of 273 kDa. It does not have any functional domains, however, its predicted secondary structure (Fig.6A´´) contains an N-

terminal β-propeller-like domain followed by α-solenoids and a clathrin-heavy-chain domain (Hirst et al., 2013) which probably mediates interaction with other proteins. *SPG11* mRNA can be detected in several tissues but it is particularly strongly expressed in the nervous system (Stevanin et al., 2007; Southgate et al., 2010). This expression pattern was also confirmed by detecting the endogenous protein by an antibody (Murmu et al., 2011). In the nervous sytem *SPG11*/SPATACSIN seems to be specific to neurons (Murmu et al., 2011; Perez-Branguli et al., 2014). Concerning the subcellular localization of SPATACSIN, upon heterologous expression a localization to the cytoplasm, the nucleus and mitochondria was reported (Stevanin et al., 2007). Endogenous SPATACSIN detected by immunostaining revealed its presence at various locations, such as microtubules, endoplasmic reticulum, γ-adaptin-positive vesicles destined for endosomal transport (Murmu et al., 2011), late endosomes/lysosomes (Hirst et al., 2013; Chang et al., 2014), or at synaptic vesicles and synaptosomes (Perez-Branguli et al., 2014).

To date, numerous studies tried to unravel the function of SPATACSIN but at present it is not yet fully understood. Knocking-down Spatacsin or Spastizin (a protein product of the *SPG15/ZFYVE26* gene associated with complex HSP) in the zebrafish results in motor impairment and abnormal branching of spinal cord motor neurons at the neuromuscular junction (Martin et al., 2012). Since knock-down of either one of these proteins did not result in an overt phenotype, whereas the partial depletion of both proteins caused motor impairment, it was suggested that both proteins might be involved in the same cellular pathway, which is consistent with the clinical similarities between these forms of HSP (Martin et al., 2012). Indeed, SPG11 co-immunoprecipitated together with SPG15, C20ORF29, DKFZp761E-198, C14ORF108, and KIAA0415 *in vitro* and was initially suggested to function in DNA repair (Slabicki et al., 2010). Later, the latter three proteins were confirmed to be the subunits of the adaptor protein complex 5 (AP-5), which is involved in specific cargo trafficking along the endolysomal system (Hirst et al., 2011). Based on secondary structure predictions, it has been speculated that Spatacsin may form a scaffold coat around AP-5 in a clathrin-like manner, while Spastizin may serve to dock AP-5 to specific membranes (Hirst et al., 2013).

Adaptor protein complexes

Adaptor protein complexes (AP) sort cargo from one vesicular compartment to another one. Structurally they represent heterotetramers each composed of two large, a medium and a small subunit. They localize to different subcellular compartments and their dysfunction is related to different diseases therefore representing a functionally important group of molecules in the cell.

To date, five different complexes have been identified (Fig.4). AP-1 sorts cargo into clathrin coated vesicles and is involved in trafficking between tubular endosomes and the trans-Golgi network (TGN) (Robinson et al., 2010). AP-1A has been shown to be essential for the lysosomal targeting and functioning of NPC1 and NPC2, two proteins mutated in the neurodegenerative lysosomal disorder Niemann-Pick type C disease (Poirier et al., 2013). AP-2 directs clathrin mediated endocytosis (Jackson et al., 2010). AP-3 sorts cargo from tubular endosomes to late endosomes/lysosomes and is related to Hermansky Pudlak Syndrome, a neurological disorder (Jones et al., 2013). AP-4 is suggested to be involved in sorting between the trans-Golgi-network (TGN) and early endosomes (Simmen et al., 2002). Loss of function mutations in subunits of AP-4 lead to cerebral palsy (Verkerk et al., 2009; Moreno-De-Luca et al., 2011) and hereditary spastic paraplegia (Najmabadi et al., 2011; Bauer et al., 2012; Kong et al., 2013), respectively. The most recently identified adaptor protein complex 5 (AP-5) is reported to localize to late endosomes/lysosomes, but its function is so far not well understood (Hirst et al., 2011). Mutations in the zeta subunit of AP-5 (AP-5ζ) lead to SPG48 (Slabicki et al., 2010). Patients suffering from SPG48 share many symptoms with SPG11 and SPG15 patients (Pensato et al., 2014).

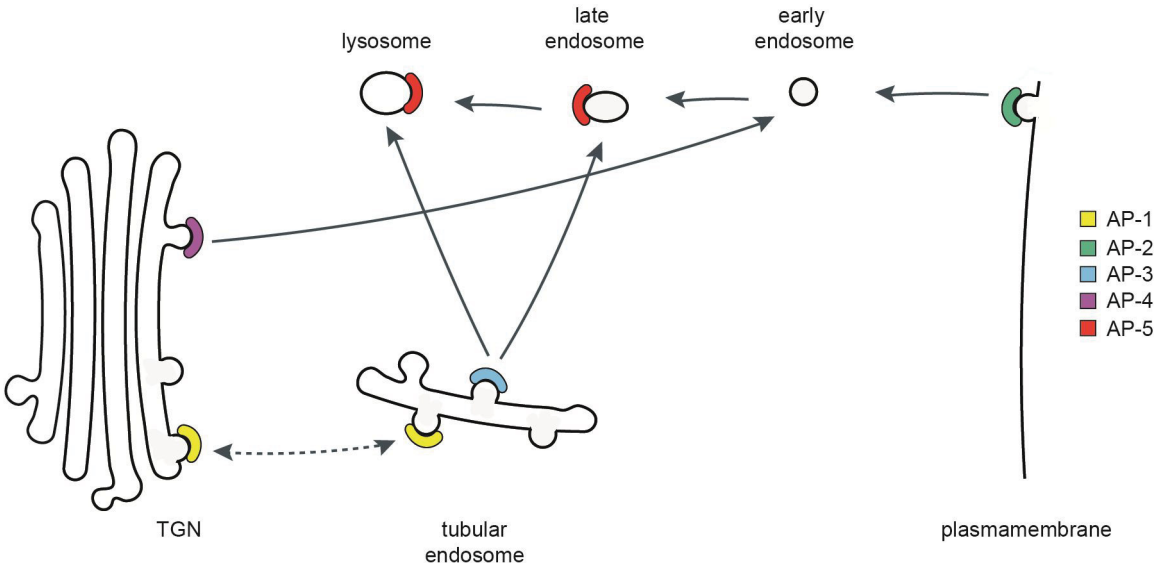

Figure 4. The role of adaptor protein complexes in the cell (based on Hirst et al., 2011.).

Autophagy

Recently, Spastizin has been shown to interact with Beclin-1 (Vantaggiato et al., 2013) a key regulator of the initial steps of autophagy. Since SPG11 and SPG15 patients manifest similar clinical phenotype and the two proteins (SPATACSIN and SPASTIZIN, respectively) encoded by these genes are predicted to function in the same pathway, therefore impairement of autophagy may be relevant for the disease phenotype.

Autophagy is a process by which cytoplasmic constituents, misfolded proteins and organelles are targeted by autophagosomes to lysosomal degradation. The first step of autophagy is the initation of a membranous structure called phagophore which sequesters cytoplasmic components. In the elongation phase this membrane extends and forms the double-membraneous autophagosome, which can then fuse with endosomes generating the so called amphisomes. These compartments can fuse with lysosomes and are then called autolysosomes in which the engulfed material is degraded (Klinonsky et al., 2011.). Lysosomes can be recycled from autolysosomes in a process called autophagic lysosome reformation (Rong et al., 2012) (Fig.5).

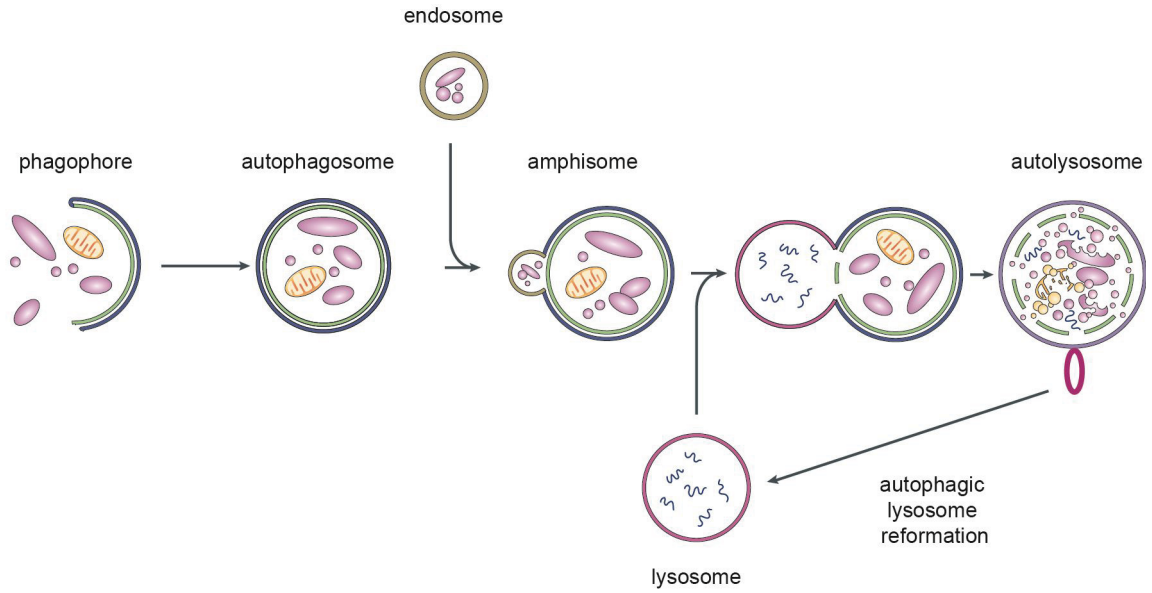

Figure 5. Autophagy (modified from Klinonsky et al., 2011.).

Phagophores are formed *de novo* by nucleation on a preexisting membrane (Abada et al., 2014). In higher eukaryotes the phagophore membrane originates from different oganelles in the cell. The phagophore formation is initiated when the ULK1-ATG13-ATG101-FIP200 and PI3KC3 (VPS34,Beclin-1,ATG14L,VPS15) complexes are recruited to curved membrane sites expressing the VMP1 transmembrane protein. This step initiates the recruitment of the ATG12-ATG5-ATG16L1 complex. The membrane bound PI3KC3 enhances membrane bending and forms a platform to recruit WIPI2 which in turn assembles more of the ATG12 complex. Activated LC3 is recruited to the membrane by the ATG12 complex, resulting in the lipidiation of LC3 at the curved membrane forming the phagophore (Carlsson et al., 2015). In the following, phagophores elongate which is a flexible process due to the size of the autophagic cargo which varies from small molecules to large bacteria and mitochondria (Stolz et al., 2014). The delivery of cargo to autophagosomes during the autophagic process is achieved by adaptor proteins as e.g. p62 (Deretic et al., 2010). Having an ubiquitin-association domain, p62 interacts with misfolded proteins and mediates aggregation in order to form condensed cargo-p62 complexes (Ichimura et al., 2010). Through its LC3-interacting domain cargo-loaded p62, delivers cargo to autophagic vacuoles (Filimoneko et al., 2010). Following cargo engulfment during the elongation process, autophagosomal biogenesis is completed. Later, amphisomes and autolysosomes are generated by the fusion with endosomes and lysosomes,

respectively. Lysosomes are digestive components in cells. They typically have a diameter >1µm and are surrounded by a single membrane. The proper functioning of lysosomes depends on soluble lysosomal hydrolases and lysosomal membrane proteins (LMPs). The degradation of intracellular components is mediated by lysosomal hydrolases (proteases, peptidases, phosphatases, nucleases, glycosidases, sulfatases, lipases). The best known proteases are the cathepsin family which include cystein proteases (cathepsins B, H, L S, C, K, O, F, W, X and V) and aspartate proteases (cathepsin D and E) (Repnik et al., 2012). Interestingly, cathepsin D dysfunction is also associated with a neurodegenerative disease (Amritaj et al., 2013). So far, more than 20 LMPs have been identified (Lübke et al., 2009), which mediate a wide range of lysosomal functions. One of the most abundantly expressed LMP is the lysosome-associated membrane protein (Lamp)-1. Lamp1 is a type-I membrane protein which is delivered to lysosomes by AP3 (Peden et al., 2004) and plays a key role in the maturation of autophagosomes.

Objectives

SPG11 is mutated in autosomal recessive HSP and encodes the protein SPATACSIN. Spatacsin has been shown to interact with the AP5 complex which is suggested to sort cargo along the endolysosomal system (Hirst et al., 2011), however, the function of Spatacsin in HSP is not yet understood. In order to obtain deeper insights into the physiological role of Spatacsin the aims of this study were the following:

1. To study the endogenous *Spg11* expression.
2. To generate a *Spg11* knockout mouse model.
3. To analyze the consequences of the absence of *Spg11* in the mouse both at systemic and cellular level.
4. To investigate if the loss of the AP5 interacting Spatacsin affects lysosomal function.
5. To asses whether autophagy is altered upon *Spg11* disruption.

Materials and Methods

Chemicals and solutions

Chemicals were purchased from Merck, Roth or Sigma unless otherwise stated. Solutions were prepared with $aqua_{bidest}$.

Bacterial Strains, vectors and Laboratory Animals

bacterial strain	Escherichia coli XL1 blue	Stratagene
vector	pCR®4-TOPO®	Thermo-Scientific
laboratory animal	*Mus musculus* (C57BL/6J)	Animal facility (SEK-FZL, Lobeda) at the University Hospital Jena

Table 1. Organisms and cloning vectors used in the study

Antibodies

Primary antibodies

For immunofluorescence studies

Commercially available:

antibody	dilution	company
mouse anti-NeuN	1:1,000	Millipore
mouse anti-GFAP	1:1,000	Millipore
rat anti-Lamp1	1:500	BD Pharmigen
rabbit anti-LC3	1:200	Sigma Aldrich
mouse anti-p62	1:250	Abcam

For immunoblot studies

Self-generated:

Monoclonal antibodies were raised against the epitope EKLSSGSISRDD (amino acids 1400-1411) of the Spatacsin protein in BALB/C mice (Abmart). The c346 anitsera were affinity-purified before use.

mouse anti-Spatacsin	1:50
rabbit anti-Spastizin	1:50

Commercially available:

rat anti-Lamp1	1:1,000	BD Pharmigen
rabbit anti-LC3	1:500	Novus Biologicals

mouse anti-p62	1:1,000	Abcam
rabbit anti-Beclin-1	1:500	Santa Cruz
goat anti-CtsD	1:500	Santa Cruz
rabbit anti-β-actin	1:2,000	Abcam
goat anti-GAPDH	1:500	Santa Cruz
goat anti Ap5b1	1:500	Santa Cruz

Secondary antibodies (all commercially available)

Fluorescence–labelled secondary antibodies for immunofluorescence studies

goat anti-mouse-Cy3	1:500	Jackson Immuno Res. Labs
goat anti-rabbit-Cy5	1:1,000	Dianova
goat anti-rat-Cy5	1:1,000	Jackson Immuno Res. Labs
goat anti-mouse-Cy5	1:1,000	Jackson Immuno Res. Labs

For the counterstaining of nuclei

Hoechst-33258	1:10,000	Molecular Probes

Horseradish peroxidase–labelled secondary antibodies for immunoblot studies

goat anti-rabbit	1:4,000	Amersham Bioscience
goat anti-mouse	1:4,000	Amersham Bioscience
donkey anti-goat	1:1,000	Santa Cruz
goat anti-rat	1:1,000	Santa Cruz

Phenotyping

All animal experiments were approved by the Thüringer Landesamt für Lebensmittelsicherheit und Verbraucherschutz (TLLV) in Germany (approval number 02-016/13).

Foot-base-angle analysis

One way to measure gait disturbances in mice is to measure the foot-base-angle at a toe-off position during walking on a beam traversing to the home cage of the animal (Irintchev et al., 2005.). Mice were trained to walk on a 1000 mm long and 40 mm wide elevated plastic horizontal beam. All animals learned to traverse the beam during two consecutive days. The following day, 5 trials for each animal were recorded by a NV-DS12 camera (Panasonic Deutschland, Hamburg, Germany). For the quantitative analysis, two individual video sequences were selected and digitized using *VirtualDub 1.5.10* (free software available at http://www.virtualdub.org). In order to quantify the foot-stepping angle single frames of digitized video sequences were analysed by the UTHSCSA *ImageTool 2.0* program (free software available at http://www.ddsdx. uthscsa.edu/dig/). The mean of two independent trials were taken for statistical analysis. Results are presented as mean ± SEM.

Beam-balance test

To estimate whether mice show sigs of ataxia, mice had to traverse a narrow elevetad plastic beam (1000 mm long and 20 mm wide) leading to the home cage. Following a training session similar to the foot-base-angle analysis, animals were video recorded. The videos were processed (see above) in order to determine the number of falls from the beam. Results are presented as mean ± SEM.

Rotarod analysis

Motor coordination was assessed by the accelerating rotating rod analysis (Ugo basile). In this excersise the animals were placed on a horizontal rod that rotates. The speed gradually increased and the latency to fall off the rod was determined, which correlates with motor skills. Mice were trained for two days before analysis.
Results are presented as mean ± SEM.

Molecular biology methods

Isolation of RNA from mouse brain tissue

Mice were decapitated and the brain was removed. The tissue was grinded under liquid nitrogen with a mortar and pestle and transferred into a 50 ml falcon. 1 ml Trizol (Invitrogen) per 100 mg tissue was added after the liquid nitrogen had evaporated. Samples were thoroughly vortexed and incubated for 5 minutes at room temperature. To pellet the cellular debris samples were centrifuged for 5 minutes at 4,000 g at 20°C. The supernatant was transferred into a new tube. 200 µl of chloroform per 1 ml Trizol was added and samples were shaken by hand for 15 seconds followed by an incubation for 2 minutes at room temperature and subsequently by a centrifugation step at 13,000 rpm at 4°C for 15 minutes. The aqueous (upper) phase was transferred into a new tube and the RNA was precipitated by adding 1 volume of isopropanol by incubation for 10 minutes at room temperature and centrifuged at 13000 rpm at 4°C for 10 minutes. The resulting RNA pellet was washed with 75% (v/v) ethanol, air dried, and carefully dissolved in RNase free water. RNA was stored at -80°C until further use.

Extraction of DNA from tail biopsies by Hot-Shot protocol

Genomic DNA was extracted from tail biopsies by a fast method called Hot-Shot extraction. Each tail biopsy (2 to 3 mm in size) was incubated in 75 µl of alkaline lysis buffer (25 mM NaOH, 0.2 mM EDTA) for 45 minutes at 95°C. After cooling down the samples on ice for 5 minutes, per probe 75 µl of neutralization buffer (40 mM Tris-HCl, pH 5.0 without adjustment) was added as the final step.

Genotyping PCR

Genotyping was performed on DNA isolated from Hot-Shot tail biopsies. The primers “for” (cggctgcgggcagtctccaagtgc), “rev” (gggatgggaaaggttccgagaggc), and “cas_rev” (cgactcagtcaatcggaggactgg) were used in a single PCR reaction. The primer pair for/rev amplified a 256 bp fragment for the wild-type allele (Fig.6A)and the primer pair for/cas_rev a 167 bp fragment for the trapped allele (Fig.6A´). Each reaction was performed in a total volume of 10 µl with 0.1 -1 µg of template, 1x of reaction buffer (Invitrogen), 10 pmol of each primer (MWG-Biotech), 0.5 mM of each dNTP’s

(Invitrogen) and 0.1 µl of Taq DNA polymerase (Invitrogen). The PCR was performed in a thermocycler with initial denaturation at 95°C for 300 seconds, 35 cycles of denaturation at 95°C for 30 seconds, annealing at 58°C for 30 seconds, elongation at 72°C for 30 seconds followed by a single step at 72°C for 180 seconds and then storage at 4°C.

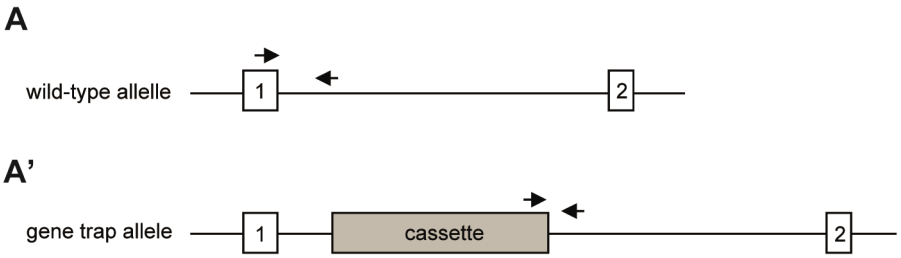

Figure 6. Genotyping strategy
(A) A 256 bp wild-type allele was amplified by a primer pair detecting a part of exon 1 and intron 1. **(A´)** A primer pair recognizing a part of the trap cassette and intron 1 amplified a 167 bp fragment for the trapped allele. arrows: location of primers, rectangles: exons, cassette: gene trap cassette.

Reverse transcription

1 µg of WT brain RNA was used to synthesize cDNA (Thermo Scientific RevertAid^{TM} First Strand cDNA Synthesis Kit) which was used as template in the Polymerase Chain Reaction (PCR) in order to amplify a 602 bp Northern blot probe (part of exon 30 of *Spg11*) with the forward primer 5'-gcaaacactaacacacactccgcagtgg-3' and the reverse primer 5'-gcaacaccagcactagatcctggc-3'. ~1µg of template, 1x of reaction buffer (Invitrogen), 10 pmol of each primer (MWG-Biotech), 0.5 mM of each dNTP's (Invitrogen) and 0.1µl of Taq DNA polymerase (Invitrogen) were used in a total volume of 25 µl. After amplification in T3000 thermocycler (Biometra) (initial denaturation at 95°C for 240 seconds, followed by 23 cycles of denaturation 95°C 40 seconds, annealing 56°C 40 seconds, elongation 72°C 60 seconds), the resulting PCR product was subsequently separated by agarose gelelectrophoresis and analyzed with UV table.

Purification DNA from Agarose Gel

For cloning DNA bands of the correct size were quickly excised under UV light from agarose gels with a scalpel and placed into a 1.5 ml tube. The DNA was purified with the DNA recovery kit (Zymoclean) according to the manufacturer's instructions.

TA Cloning

Following the extraction of the PCR product, the 602 bp fragment was cloned into a TOPO vector. The mix included 2µl of gel-purified cDNA, 1µl of Salt Solution (Invitrogen), 2µl water and 1µl of TOPO vector (Invitrogen). After mixing the reaction gently, it was incubated for 20 minutes at room temperature and then transformed into chemo-competent bacteria.

Preparation of chemo-competent bacteria

For the preparation of chemo-competent bacteria a preculture of E. coli XL1 Blue (Stratagene) was grown overnight at 37°C in 2 ml ψ broth medium (LB-broth medium, 4 mM $MgSO_4$, 10 mM KCl, 3 µg/ml tetracycline adjusted to pH 7.0 and autoclaved). The next morning, 500 ml ψ broth medium was inoculated with 1 ml of the preculture and grown at 37°C and was shaken until an optical density of 600 nm (OD600) of 0.3-0.6 was reached. Bacteria were cooled on ice and then pelleted by centrifugation at 3,000 rpm for 5 minutes at 4°C. The supernatant was discarded and the pellet was resuspended in 150 ml ice-cold TFB1 buffer (15% (v/v) glycerol, 10 mM $CaCl_2$, 30 mM potassium acetate, 100 mM RbCl, 50 mM $MnCl_2$, pH 5.8 adjusted with CH_3COOH) and incubated on ice for 60 minutes. After this step the bacterial suspension was centrifuged at 3,000 rpm for 5 minutes at 4°C. The supernatant was discarded and the pellet was resuspended in filtered sterile, ice-cold TFB2 buffer (15% (v/v) glycerol, 10 mM MOPS, 75 mM $CaCl_2$, 10 mM RbCl). Competent cells were quickly aliquoted on ice (50 µl) and snap-frozen in liquid nitrogen and stored at -80°C until use.

Transformation of competent bacteria

The plasmid DNA was mixed with a defrosted aliquot of chemo-competent bacteria for transformation and incubated on ice for 20 minutes. Transformation of the plasmid was done by heat shock at 42°C for 2 minutes. After cooling on ice for 2 minutes,

250µl of SOC medium (0.5% (w/v) yeast extract, 2% (w/v) tryptone, 10 mM NaCl, 2.5 mM KCl, 10 mM $MgCl_2$, 10 mM $MgSO_4$, 20 mM glucose, pH 7.0) was added and the mixture was incubated at 37°C on a shaker for 60 minutes. The bacterial suspension was plated on LB-Agar plates containing the appropriate antibiotic for plasmid selection. Inverted plates were incubated at 37°C overnight

Bacterial liquid culture

After successful transformation, a single bacterial colony was inoculated in 3 ml of LB containing 50 mg/ml of kanamycin in a sterile culture tube. The culture was grown overnight at 37°C with shaking (180 rpm).

Mini preparation of Plasmid DNA Bacterial Clones

1.5 ml of the culture was transferred to a tube. Bacteria were pelleted by centrifugation and resuspended in 100 µl of P1 buffer (50 mM glucose, 25 mM Tris-HCl pH 8.0, 10 mM EDTA, 100µg/ml RNase A). Alkaline lysis of the bacteria was performed by adding 200 µl of P2 buffer (200 mM NaOH, 1 % (w/v) SDS) and gently mixing the tubes by inversion. After a brief incubation on ice, 150 µl of P3 buffer (5.0 M Potassium Acetate, pH 4.8) was added and the tubes were gently inverted five times in order to be mixed. Removal of the precipitated proteins from the lysate was achieved by a 5 minutes centrifugation at 14,000 rpm. The supernatants were transferred into new 1.5 ml tubes and 900 µl of 100 % (v/v) ethanol was added for plasmid DNA precipitation. Following centrifugation at 14,000rpm for 5 minutes, DNA pellets were washed with 70 % (v/v) ethanol, allowed to dry, and dissolved in water.

DNA Sequencing

DNA was sequenced in order to verify the nucleotide sequence of the cloned plasmid DNA. A sequencing reaction included 100-500 ng DNA template, 10 pmol sequencing primers (MWG-Biotech), 2 µl 5x buffer, 1 µl of Big Dye (ABI) and H_2O in a total volume of 10 µl. The mix was amplified in a thermo-cycler with the following sequencing program: initial denaturation at 96°C for 60 seconds, denaturation 96°C 10 seconds, annealing 55°C 8 seconds, elongation 60°C 240 seconds. Subsequently, the DNA was precipitated by adding 1/10 vol. of 3M sodium acetate (pH 5.2) and 2.5 vol. of ethanol and was centrifuged for 10 minutes at 14000 rpm.

After washing it with 70% (v/v) ethanol, the pellet was dried and solved in 10µl of Hi-Di™ Formamide (ABI) and was processed for sequencing. Chromatograms were analyzed by *GATCViewer* (free software at gatcviewer.software.informer.com).

Agarose Gel Electrophoresis

Separation of DNA fragments from the genotyping PCR was achieved by horizontal gel electrophoresis in agarose gel chambers (Amersham Bio-Sciences). Agarose gel concentration was 1-2 % (w/v) depending on the size of the DNA fragments to be separated. Agarose (Invitrogen) was boiled in 1x TAE buffer (40 mM Tris-acetate, 1 mM EDTA). Before casting, 0.5 µg/ml ethidium bromide was added to the gel. DNA samples were mixed with 6x DNA loading buffer (10 mM Tris-HCl, 30% (v/v) glycerol, 0.25% (v/v) bromophenol blue, 0.25% (v/v) xylene cyanol) in order to monitor the DNA separation. The DNA fragments were separated by applying a constant voltage of 100-150 V depending on the separation time. After separation the DNA was visualized under UV light.

Northern blot

In order to analyze the *Spg11* mRNA expression by Northern blot analysis we used the previously extraced brain RNA and a probe directed against a part of exon 30 of *Spg11*. 25 µg RNA isolated from wild-type and homozygous knockout mouse brain was denatured in RNA-loading buffer (5x RNA loading dye: 0,25 (v/v) % bromophenol blue, 4 mM EDTA, 0,9 M formaldehyde, 20 % (v/v) glycerol, 30,1 % (v/v) formamid, 4x MOPS) at 65°C for 10 minutes. Denaturated RNA samples were loaded on an agarose gel (1 % (w/v) agarose, 7 % (v/v) formaldehyd, 1x MOPS) for electrophoresis. 10x MOPS stock solution (200 mM 3-(N-morpholino) propanesulfonic acid, 50 mM sodium acetate, 10 mM EDTA, pH 7.0). Electrophoresis was performed in running buffer (1x MOPS, 3,5 % (v/v) formaldehyde in DEPC-water) at 120 V. After separation the gel was washed twice with 10x SSC (1,5M NaCl, 0,15 M Na-Citrate, pH 7.0) for 30 minutes. RNA was blotted onto a nylon membrane (Hybond-XL, GE Healthcare) in 10x SSC overnight by capillary blotting. RNA was fixed onto the membrane by incubating it at 80°C for 2 h. The integrity of the transferrred RNA was monitored by methylene blue staining (equilibration of membrane in 5 % (v/v) acetic acid and stained with 0.01 % (w/v) methylene blue in

5 % (v/v) acetic acid for 30 minutes, followed by destaining of the membrane with H_2O). The presence of the 18S-rRNA and 28S-rRNA bands served as a marker for the successful blotting and equal loading of different lanes. The membrane was equilibrated in 2x SSC and stored at 4°C until hybridization.

Radio-labeling of the probe

The Northern blot probe for hybridization of the Nortern blot membrane was labelled with 32P-dCTP. The 602 bp probe template was excised from the plasmid with EcoRI (Invitrogen), gel purified and dissolved in TE buffer at a concentration of 25-50 ng / 45 µl. After denaturing the sample at 95°C for 5 minutes, it was cooled down on ice and briefly centrifuged. The denatured probe template was transferred into a Rediprime II (GE Healthcare) tube containing lyophilized dATP, dTTP, dGTP and DNA polymerase. The lyophilized Rediprime II components were mixed and then 5 µl of 32P-dCTP was added and mixed again by pipetting. The reaction was incubated for 30 minutes at 37°C. In order to remove the unbound radiolabelled nucleotides, the probe mix was purified through a G50 column (GE Healthcare). A scintillation counter (Beckman) was used to test the radiolabelling of the probe. Prehybridization of the membrane was performed for 2 hours at 68°C in prehybridization mix (7% (w/v) SDS, 10% (v/v) PEG, 1.5x SSPE, 0.1 mg/ml fish sperm DNA (Roche)) in order to block nonspecific binding of the probe with the membrane. Hybridization with the radio-labelled probe was performed overnight at 68°C in rotating bottles. The membrane was washed twice with preheated wash buffer (2x SSC, 0.1% (w/v) SDS) at 68°C for 20 minutes. The membrane was washed until radioactivity was below 200 cpm, then it was wrapped into saran and exposed to a Phospho-imager plate (FujiFilms). The FLA-3000 phospho-imager (FujiFilms) was used to read the phosphoimager plates after a suitable exposure time.

Cell biology methods

Mouse embrionyc fibroblast culture

In order to get 13.5 days old embryos, terminated matings were set up. The pregnant female mice were euthanized at day 13.5 after conception and embryos were removed. Embryos were placed in a dish filled with sterile 1x PBS on ice. Extra blood was removed by washing with PBS. By using a sharp forceps the uterine wall and the amniotic sac was removed from the embryo. The embryo was fixed with forceps while the inner organs, eyes, brain and limbs were removed. The remaining of the embryo was minced with a scalpel in Embryo-Suspensions-Medium (DMEM Hepes (Invitrogen), 5000 units / ml penicillin, 5000 µg / ml streptomycin (100X penicillin/streptomycin, (Invitrogen)). To break up tissue chunks and get cells into suspension the minced tissue was taken up in 2 ml of Embryo-Suspensions-Medium and passed through needles of decreasing calibers in order to get a smooth suspension. Finally the cell suspension was transferred into 15 ml Falcons and 5 ml 0,05% Trypsin (Gibco) and 50 µl Dnase (Gibco) was added to the suspension. After mixing well the sample, it was incubated for 10 minutes at 37°C in watherbath. During incubation the sample was mixed from time to time. Following 2 minutes of settling time on room temperature 5 ml of supernatant was pipetted into a 50 ml falcon with 20 ml MEF-P0-Medium (DMEM Hepes (Invitrogen), 15% (w/v) FCS (PAA gold), 1% (w/v) NEAA (non essential amino acid, 100x) (Invitrogen), 5000 units/ml penicillin, 5000 µg/ml streptomycin (100X penicillin/streptomycin, (Invitrogen)), 1% (w/v) Glutamin). The trypsination step was repeated four times. The resulting 40 ml of cell suspension was centrifuged for 10 minutes at room temperature by 1,100 rpm. The pellet was resuspended in fresh medium and the cells were plated on 10 cm dishes at a densitiy of $1{,}5x10^5$/ml in MEF culture medium (MEF culture medium (DMEM Glutamax-I, 4500 mg/l glucose, sodium pyruvate-free medium (Invitrogen), 9% (w/v) heat-inactivated FCS (PAA gold), 1% (w/v) NEAA (Invitrogen), 5000 units/ml penicillin, 5000 µg/ml streptomycin (100X penicillin/streptomycin, (Invitrogen)).

Starvation assay

When MEFs were starved in MEF medium lacking serum (serum starvation) for 0, 6 and 14h after reaching a confluency of roughly 70%.

Blastocyst injection and generation of chimeric mice

Frozen 129/E14Tg2 embryonic stem (ES) cells were defrosted and mixed with 200 µl of prewarmed E14Tg2a medium (500 ml GMEM, 50 ml FBS (Invitrogen), 5 ml 100x GIBCO L-Glutamine (Invitrogen), 5 ml 100x beta-mercaptoethanol, and Murine LIF (Milipore)). ES cells were grown on cell culture dishes carrying a thin coat of 0.1 % gelatine. Blastocysts were removed from pregnant C57BL/6J females 2-3 days after fertilization. ES cell clones were trypsinized, washed twice with 5 ml of PBS and added to 500 µl E14Tg2a medium. 10-15 ES cells were injected into each blastocyst (C57BL/6J mouse line) using a micromanipulator (Eppendorf). Blastocysts carrying the recombinant ES cells were injected via a capillary into the uterus of anesthetized pseudo-pregnant females, which gave birth to chimeric mice. Chimeras were mated with C57BL/6J mice to obtain heterzygous offsprings. The ES cell culture and the blastocyst injection was performed in the Core Unit of the Animal Facility of the University Hospital Jena.

Perfusion and fixation

For the histological analysis mice of different ages were anesthethised by Isoflurane (Actavis) and perfused transcardially. To remove blood 1x phosphate buffered saline (PBS: 140 mM NaCl, 3.2 mM Na_2HPO_4, 2.7 mM KCl, 1.5 mM KH_2PO_4; pH 7.4) was used. After blood was removed tissues were fixed with fixation buffer as suited for the planned experiments. We applied for β-galactosidase stainings a β-galactosidase fixing solution (for 10 ml soltution: 0,27 ml 37 % formaldehyde (Fluka Chemie GmbH), 0,08 ml 25 % glutaraldehyde, 1 ml 10 x PBS, ad $aqua_{bidest}$), for histological stainings and immunohistochemistry 4 % (w/v) paraformaldehyde (PFA) in 1x PBS, and for ultrastructural analysis 4 % (w/v) PFA, 1% (v/v) glutaraldehyde in 1x PBS. Tissues were post-fixed for 2 h (β-galactosidase staining) or overnight in the respective fixing soltuion at 4°C.

Tissue sectioning

For β-galactosidase stainings, sagital brain sections of 100 µm were prepared by a vibratome (Leica Microsystems). For histological stainings, tissue was embedded in paraffin and sectioned (8 µm) with a microtome (HM 355 S, Waldorf) and transferred onto HystoBond+ slides (Marienfeld). For immunohistochemistry, samples were cryoprotected in an increasing concentration of sucrose solution (10 and 30 % sucrose in 1x PBS) for 4 h and overnight. 40 µm sections were cut with a sliding microtome (Leica) and floating sections were stored in 1x PBS supplemented with 0.025 % NaN_3 until further use. For ultrastructural analysis, 150 µm sagital and coronal sections of brain and spinal cord were cut with by a vibratome (Leica Microsystems).

β-galactosidase staining

In order to analyze the endogenous expresion pattern of *Spg11*, the brain was removed from 3-month-old heterozygous animals and sectioned after post-fixation. Sections were washed with 1x PBS for 3 times 10 minutes and incubated overnight in Lac-Z staining solution (for 10 ml solution: 0,25 ml 40 mg/ml X-Gal (Carl Roth), 0,1 ml 500 mM $K_3Fe(CN)_6$, 0,1 ml 500 mM $K_4Fe(CN)_6$, 0,1 ml 200mM $MgCl_2$ 1 ml 10x PBS, 0,2 ml 10% (v/v) Triton X-100, ad $aqua_{bidest}$). After the staining, samples were washed 3 times 10 minutes in 1x PBS and were mounted (Fluoromount, Southern Biotech). All samples were analysed by a digital stereo microscope (VH-Z100R - Keyence).

Hematoxilin and Eosin (HE) Staining

The 8 µm paraffin sections were deparaffinized for 2 x 10 minutes in xylol and rehydrated in decreasing concentrations of ethanol (100 %, 96 %, 80 %, 70 %, 50 % (v/v) each time 2 minutes). This step was followed by shortly rinsing the samples in $aqua_{bidest}$. Samples were incubated in hematoxilin (Carl Roth) for 15 minutes. In order to let the color develop sections were washed for 10 minutes in warm running water and then stained with eosin (Carl Roth) for 20 seconds. Tissue sections were dehydrated by increasing concentrations of ethanol (80%, 96%, 100% (v/v) each for 2 minutes) and finally washed in xylol 2 times for 5 minutes each. Samples were embedded using entellan. For the quantification of Purkinje cells, images were taken with the Zeiss Axioskop 40 microscope. Purkinje cells were counted using the cell

counter plugin of the *ImageJ* software (National Institutes of Health, Bethesda). For statistical analysis the number of Purkinje cells per 1,000 µm length of the Purkinje cell layer was averaged (mean ± SEM). 3 mice per genotype were analyzed and 3 sections of cerebellum per mice were taken for the statistical tests.

Nissl staining

In order to visualize brain structures cresyl violet staining was used on 8 µm sections. Following deparaffinization and rehydration (as seen above: HE staining). Sections were stained with prewarmed 0,1% cresyl violet for 20 minutes. After rinsing in 1x PBS, sections were dehydrated and washed in Xylol for 5 minutes each and finally embedded by entellan. Images were captured with an Olympus DP70 microscope.

Immunohistochemistry

Brain and spinal cord

Free-floating brain and spinal cord cryosections (40 µm) were taken to perform immunhistochemical stainings. Sections were washed 3 times 10 minutes in 1x PBS, then tissues were permeabilized by PBS with 0.25 % Triton X-100 for 1x 20 minutes. In order to avoid unspecific staining, tissues were incubated in a blocking solution (5 % normal goat serum (Millipore) in wash buffer (1x PBS with 0.25 % Triton X-100)) for 1h at room temperature. Slices were stained with the primary antibody diluted in blocking solution overnight at 4°C. Then samples were washed with wash buffer for 3 times 15 minutes. After incubation with the secondary antibody in blocking solution for 1h at room temperature, samples were washed again, stained with Hoechst-33258 (0,1 µg / ml) to visualize nuclei and mounted. Further analysis was performed by confocal microscopy (TCS SP5, Leica).

For the quantification of neurons in the motor cortex sagittal brain sections were stained for the neuronal marker NeuN. Images of the motor cortex of wild-type and knockout brains were taken at comparable positions. Between genotypes and samples, all parameters were kept constant including the z-Stack (8 optical sections in a z-volume of 40 µm), speed of scan (100Hz), detector gain of 720 V. Maximum projection intensity images, calculated with the help of *ImageJ* software were exported as TIFF formats and neurons per area were counted. Statistical analysis

was obtained from 3 animals per genotype, and the results are presented as mean ± SEM. Gliosis was analyzed using a mouse anti-GFAP antibody on 40 µm sagittal brain and coronal spinal cord sections.

To characterize the cellular origin of the autofluorescent material, spectral analysis on brain sections was performed at the Biomolecular Photonics Group of the University of Jena. Samples were stained against the rat anti-Lamp1, mouse anti-p62 or rabbit anti-LC3 respectively. In each case we used secondary antibodies coupled to Cy5. Fluorescence images were recorded by a confocal laser scanning microscope (LSM710, Carl Zeiss Jena). Autofluorescence was excited with the 488 nm line of an argon ion laser. The Cy5 tag of the secondary antibodies was excited with the 633 nm line of a He/Ne Laser. Fluorescence emitted from the sample was recorded with the spectral detector of the microscope in the wavelength range from 501-725 nm. Unstained samples were used as controls to substract background. The colocalization of the Cy5 dye with the autofluorescence components was determined by a linear unmixing algorithm (Dickinson et al., 2001; Zimmerman et al., 2003). The number of lysosomes defined as Lamp1 positive and p62 negative vesicles was quantified in Purkinje cells. Three mice per genotype and 20 cells per mice were used for the quatification. Only sections of somata of Purkinje cells not extending beyond the image boundary and hit vertically with respect to the nucleus were selected. The number of free lysosomes was calculated and normalized to the area of the cell soma with *ImageJ* and results are shown as mean ± SEM.

MEFs

Cells were fixed in 4% PFA for 15 minutes on room temperature, then rinsed briefly for 3 times with 1x PBS, followed by permeabilizing for 15 minutes at room temperature in 1x PBS supplemented with 0,02% TritonX. For blocking 1% goat serum in 1x PBS / 0,02% Triton X was used for 1h at room temperature. The primary and secondary antibodies were dissolved in blocking solution as written above and Hoechst-33258 was used to stain nuclei. Between the antibody stainings 3 washing steps were included with 1x PBS / 0,02% TritonX. Finally coverslips were mounted and analysed by TCS SP5 confocal microscope (Leica). The quantification of free lysosomes in MEFs was done similiarly to Purkinje cells. For the analysis 3 coverslips per genotype and 5 cells per coverslips were used for each time point. Co-

localization between Lamp1 and p62 was determined in *BioImageXD* (free software www.bioimagexd.net*)* as previously described (Kankaanpaa et al., 2012).

Intralysosomal pH measurement

Lysosomal pH measurements were carried out as described previously (Weinert et al., 2010). More than 1,000 lysosomes from 3 independent experiments were analysed per genotype.

Ultrastructural analysis

The Electron Microscopy Center of the University of Jena provided the facility for the ultrastructural analysis. The 150 µm sections of brain and spinal cord were washed with PBS for 3 times 10 minutes. After washing three times with cacodylate buffer (0.1 M, pH 7.4), samples were post-fixed with 1% (w/v) osmium tetroxide in cacodylate buffer. Next, in ascending ethanol series staining with 2% (w/v) uranyl acetate was done. After embedding in araldite, semithin sections (1 µm) were prepared with a glass knife using an ultramicrotome and stained with toluidine blue (1% (w/v) toluidine blue, 2% (w/v) borate in $aqua_{bidest}$) for light microscopic orientation, and 80 nm ultrathin sections were cut using a diamond knife and finally stained with lead citrate in order to get an appropriate contrast of cellular structures. The samples were investigated using a EM 900 (Zeiss) transmission electron microscope.

In order to quantify large diameter axons, images were captured with an Olympus DP70 microscope. Large axons were defined as having a diameter larger than 4 µm. These axonal structures were counted per genoptypes (n=3) and results are shown as mean ± SEM.

Protein biochemistry

Protein extraction

Brain tissue lysates were prepared for western blotting with an Ultra-Turrax T8 tissue homogenizer (IKA-WERKE, Germany) in homogenization buffer (300 mM Tris-HCl pH 8.8, 5 mM EDTA, 3 mM NaF, 10 % (v/v) Glycerol, 3 % (w/v) SDS, and complete protease inhibitor (Roche)). Homogenates were centrifuged at 1,500 *g* to remove

nuclei and insoluble debris. For detecting p62, Triton-X 100 insoluble fractions were prepared as previously described (Kollman et al., 2012). Protein concentration was determined by the bicinchoninic acid protein assay (Pierce) and the Nanodrop photometer (Biotechnologie GmbH). Protein concentration was adjusted with the appropriate sample buffer. Laemmli buffer (63 mM Tris-HCl, 10 % (v/v) glycerol, 2 % (w/v) SDS, 0.0025 % (v/v) bromphenol blue, 1 % (v/v) ß-mercaptoethanol) was added and samples were denatured for 5 minutes at 95°C.

Immunoblotting

For immunoblotting, 30-80 µg of protein was separated by reducing SDS 6-8% polyacrylamide gel electrophoresis and transferred onto PVDF membranes (Roche). After blocking (2.5 % (w/v) non-fat dry milk powder, 2.5 % (w/v) BSA in TBS-T (137 mM NaCl, 2.7 mM KCl, 19 mM Tris base, 1 % (w/v) Tween)) for 1 h at room temperature, blots were incubated with the respective primary antibodies (over-night, 4°C). Detection was achieved using peroxidase-coupled secondary antibodies (2 h, room temerature) applying the ECL Plus Western Blotting Detection System (GE Healthcare) on a LAS 4000 system (GE Healthcare). For the detection of Spatacsin antibody the Super Signal Western Blot Enhancer Kit (Thermo Scientific) was utilized. Densitometry in *ImageJ* was used for quantifying band intensity.

Statistics

When comparing of two experimental groups, the un-paired parametric two-tailed Student's t-test was used. For repeated measurements in order to compare between genotypes two-way ANOVA followed by Bonferroni *post-hoc* test was applied. Significance was considered at p-values <0.05 (* indicates $p<0.05$; ** indicates $p<0.01$; *** indicates $p<0.001$).

Results

Generation of constitutive Spatacsin knockout mice

In order to study the physiological role of SPG11 *in vivo*, we created a genetrap based knockout mouse model. We selected the EUCE0085_F05 ES cell clone from the European conditional mouse mutagenesis program (EUCOMM) harbouring a genetrap cassette in the first intron of the *Spg11* gene (Fig. 7A). The gene trap cassette consists of a 5' splice acceptor site (SA), a promoterless reporter gene (βgeo) and 3' polyadenylation site (pA) (Fig. 7A´). The predicted transcript encodes a fusion protein consisting of the N-terminal part of *Spg11* and ßgeo (Fig. 7A'''). The ES cell clone was injected into donor blastocysts, which were then implanted into pseudopregnant foster mothers. The resulting chimeras were mated with C57Bl6 wildtype (WT) animals. Heterozygous offspring was subsequently mated in order to generate homozygous knockout mice. Offsprings were born in the expected Mendelian ratio and the presence of control and mutant genotypes in the F2 generation was confirmed by genotyping PCR (Fig. 7B). As expected Northern Blot analysis using a probe targeting a part of exon 30 of *Spg11* detected a 7.6 kb transcript in RNA isolated from wild-type brain tissue which was absent from knockout samples (Fig. 7C).

Validation of the anti-Spatacsin antibody

To detect the Spatacsin protein we generated a monoclonal antibody directed against an epitope within the α-solenoid domain of Spatacsin (Fig. 7A'' arrowhead) and affinity-purified the resulting antiserum. The antibody detected a band of the expected size of Spatacsin of roughly 270 kDa in control samples, which was absent in knockout tissue lysates (Fig. 7D).

Expression analysis of Spatacsin interacting partners

To asses whether the expression levels of Spatacsin interacting partners like Spastizin and the ß-subunit of the AP-5 complex (Hirst et al., 2011) are altered upon *Spg11* disruption brain protein lysates were used. Spastizin levels were reduced in brain lysates of Spatacsin knockout mice, while the levels of the of the AP-5 complex (Ap5b1) were not changed (Fig. 7E-G) in knockout samples.

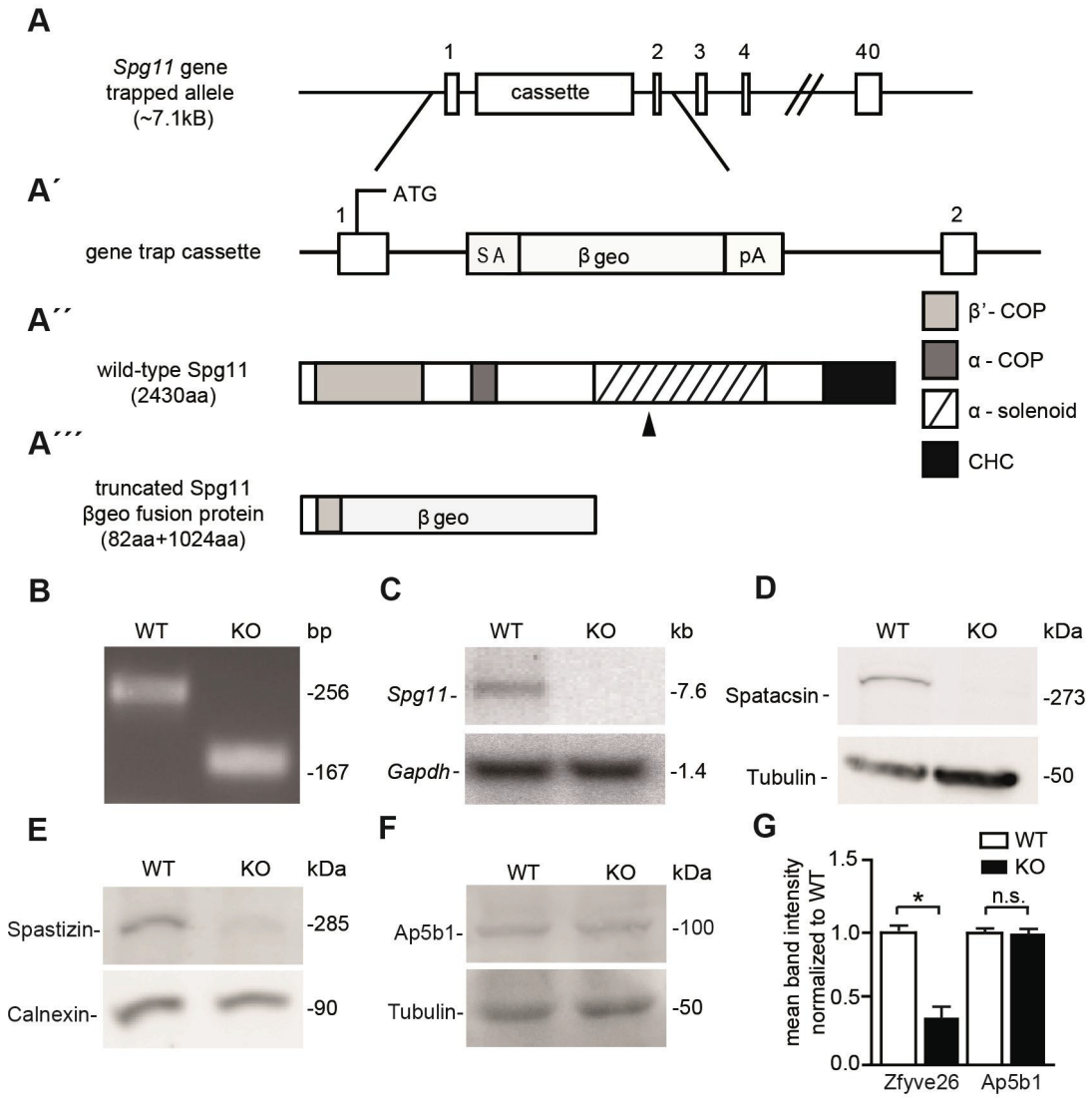

Figure 7. Homozygous trapped mice represent Spatacsin knockout mice
(A) Partial genomic structure of the targeted *Spg11* locus; rectangles: exons **(A´)** The structure of the gene trap cassette; ATG: start codon, SA: splice acceptor, βgeo: β-galactosidase and neomycin fusion cassette, pA: polyadenylation site. **(A´´)** Predicted secondary structure of WT Spatacsin; arrowhead: position of antibody epitope. **(A´´´)** The *Spg11*/ßgeo fusion protein. **(B)** PCR identifies a 256 bp WT and a 167 bp KO allele. **(C)** Northern blot analysis with a probe directed against exon 30 of *Spg11* of total brain RNA from wild-type (WT) mice detects a 7.6 kb transcript in WT, which is absent in RNA isolated from homozygous trapped mice (KO). *Gapdh* served as a loading control. **(D)** Western Blot analysis with an affinity-purified monoclonal antibody directed against the deleted part of the Spatacsin protein (the position of the epitope is indicated in (A´´) by an arrowhead) shows a band of the predicted size in WT brain lysates, which is absent in brain lysates of homozygous trapped mice. Tubulin served as a loading control. **(E-F)** Immunoblot analysis of Spastizin reveals that its leveles are diminished in brain (E), whereas levels of the beta subunit of the AP-5 complex (Ap5b1) are not changed (F). **(G)** Quantification of immunoblots show siginificant decrease of Spastizin in knockout samples while Ap5b1 were unchanged (n=3; Student's t-test: * indicates $p<0.05$; n.s.: not significant

Expression of *Spg11* in the murine nervous system

The expression of the fusion protein encompassing the ßgeo cassette under control of the endogenous *Spg11* promoter was used to study *Spg11* expression by LacZ stainings. Lac-Z staining on tissue sections of heterozygous trapped mice revealed a neuronal expression pattern of *Spg11.* Lac-Z signals were detected in cortical neurons (Fig. 8A), spinal cord neurons (Fig. 8B), and cerebellar Purkinje cells (Fig. 8C), which were absent in tissues of wild-type mice.

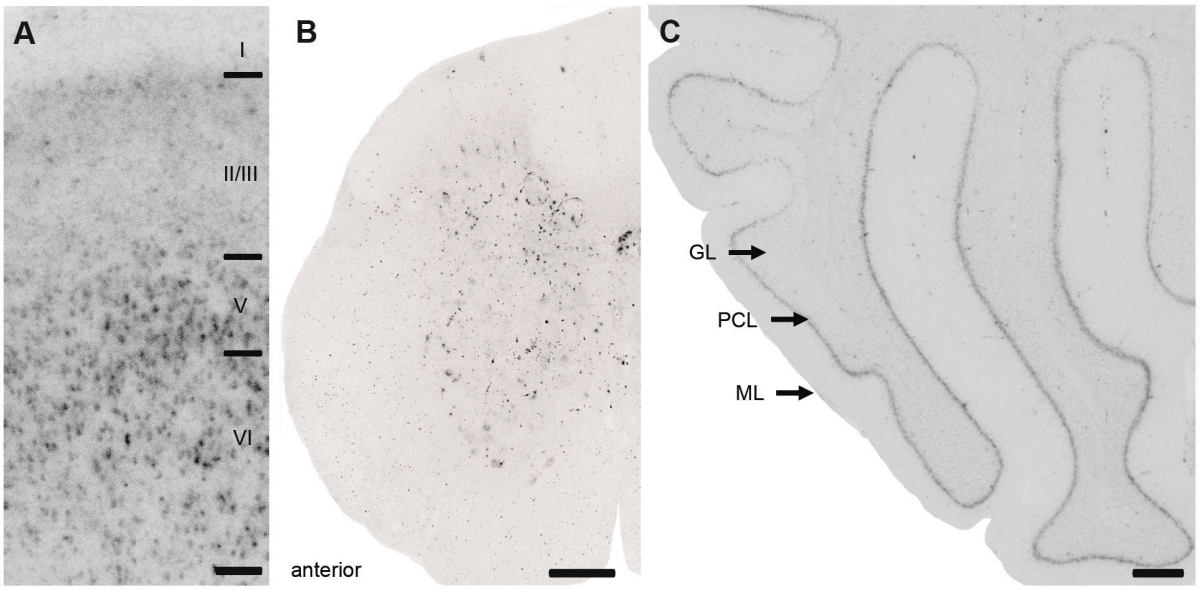

Figure 8. *Spg11* expression

LacZ stainings of tissue sections from 2-month-old heterozygous trapped mice reveals that *Spg11* expression follows a neuronal pattern including cortex (A), spinal cord (B), and cerebellum (C). Cortical layers are labeled I–VI. GL: granular layer, PCL: Purkinje cell layer, ML: molecular layer. Scale bars: 500 µm.

Spatacsin knockout mice develop a progressive gait disorder with ataxia

As compared to WT littermates, no evident phenotype was observed in Spatacsin KO mice younger than 12 months of age. Knockout mice were viable, fertile and they did not show any difference in size or weight (Fig. 9F) until 12 months of age, when the motor phenotype started to evolve. Mutant anmials developed a progressive gait disorder with ataxia paralleled by weight loss and an abnormal kyphotic posture, although their overall survival did not differ from control mice (data not shown). Motor coordination was addressed by an accelerating rotating rod analysis. Our results revealed that aged *Spg11* knockout mice fell off the rod significantly earlier as comapred to wild-type controls (Fig. 9D). To quantify the gait abnormality we also analysed the foot base angle (FBA) of the hindpaws at toe-off position (Irintchev et

al., 2005). This is measured during the beam walking test: Mice are trained to traverse a 4 cm thick beam in order to reach their home cage while they are video recorded. The gait deficit manifested at 12 months of age, when the FBA flattened (Fig. 9A-C).To study ataxia we used the beam balance test. This task is performed on a 2 cm thin beam which the mice has to traverse and the number of slips and falls are quantified. Aged knockout mice fell off the beam more frequently than wild-type littermates (Fig. 9E).

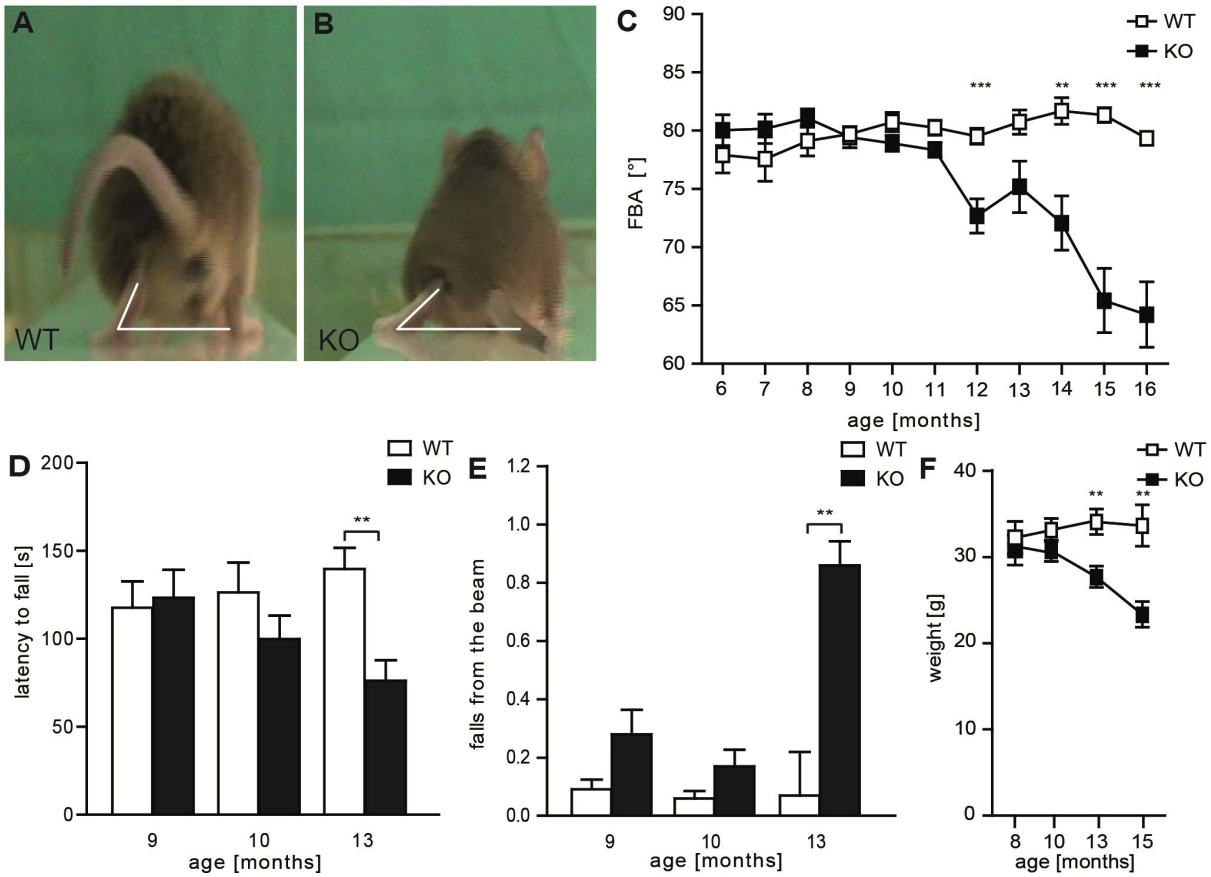

Figure 9. Spatacsin knockout mice have a severe spastic and ataxic gait disorder
(A-B) Single video frames of a WT (A) and KO (B) mouse at 14 months of age walking on a beam at the moment when the toe of the hind limb is taken off. The foot-baseangle (FBA) is indicated by white lines. **(C)** Progressive decrease of FBA over time in KO but not in WT mice (n=20; 2-way-ANOVA: $p<0.0001$; Bonferroni post-hoc analysis: *** indicates $p<0.001$ and ** $p<0.01$). **(D)** The latency to fall off an accelerating rotating rod declines over time in KO mice (n=20; 2-way-ANOVA: $p=0.05$; Bonferroni post-hoc analysis: ** indicates $p<0.01$). **(E)** Old KO mice fall off the beam more frequently than control mice (n=20; 2-way-ANOVA: $p=0.0157$; Bonferroni post-hoc analysis: ** indicates $p<0.01$). Error bars represent SEM. **(F)** Spatacsin KO mice lose body weight starting around 12 months of age. (n=20; 2-way-ANOVA: $p<0.0001$; Bonferroni post-hoc analysis: *** indicates $p<0.001$ and ** $p<0.01$).

Cortical motoneurons and Purkinje cells are progressively lost in Spatacsin knockout mice

At 16 months of age the size of the brain (Fig. 10A-B) was reduced compared to WT which was most evident at the cortex and cerebellum. Suggesting a systemic neurodegenerative disorder, this difference was not present at 2 months of age when the overall structure of the brain of knockout mice was unaltered. In order to investigate whether long projection motorneurons degenerate upon disruption of *Spg11*, the number of NeuN-positive neurons in deep cortical layers V and VI of the motor cortex was quantified (Fig. 10D-E). While it was significantly reduced at 16 months of age (Fig. 10F) this difference was not detected between genotypes in samples from 8 month old mice. Neuron numbers in layers I-III, where most of the commissural neurons reside (Greig et al., 2013), were unchanged (Fig. 10F). Consistently, the size of the corpus callosum was not different in aged knockout mice (Fig. 10G-H). Because of the ataxia and the cerebellar atrophy in aged knockout mice we also assessed the cerebellum. Indeed, histological investigation of the cerebellum disclosed that Purkinje cells (Fig. 10I-J) were almost completely absent in 16 month old knockout mice, whereas in 2 month old animals the number of Purkinje cells was unchanged (Fig. 10K).

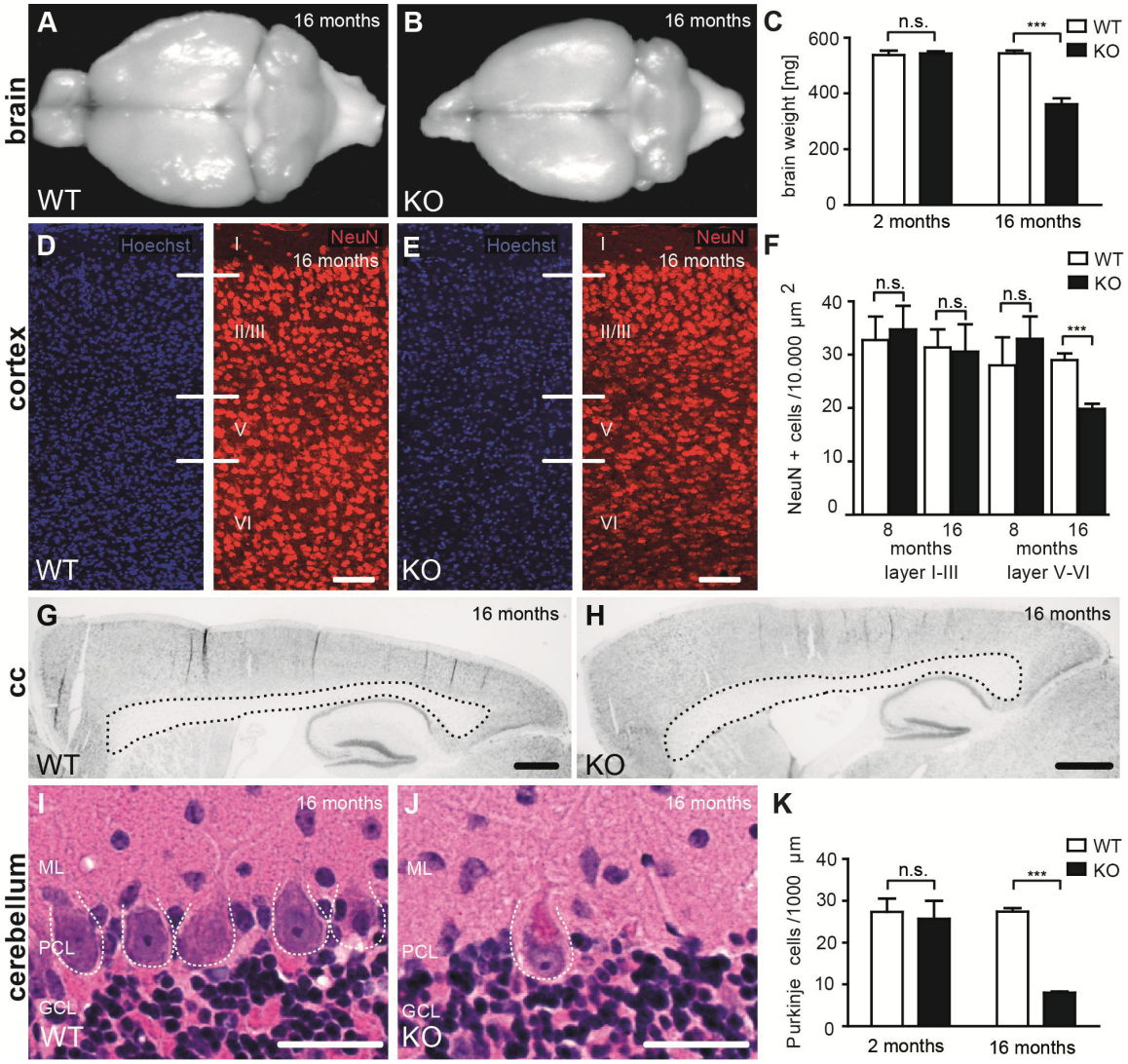

Figure 10. Spatacsin knockout mice display severe neuron loss in the motor cortex and the cerebellum

(A-B) Brain size is reduced in 16-month-old KO compared to WT mice. Scale bars: 2 mm. **(C)** Progressive reduction of brain weight in KO mice (n=3; Student's t-test: *** indicates $p<0.001$). **(D-F)** Neuron loss in the motor cortex of 16-month-old KO mice. Hoechst-33258 (blue; nuclei) and NeuN (red; neuronal marker) staining of the motor cortex at 16 months of age from WT (D) and KO (E) mice. Individual cortical layers are labeled (I–VI). Scale bars: 100 µm. Quantification of NeuN-positive cells (F) reveals a depletion of neurons from layers V-VI but not layers I-III of the motor cortex at 16 months of age in the KO (Student's t-test: *** indicates $p<0.001$). **(G-H)** Nissl stainings of sagittal brain sections do not support a thinning of the corpus callosum of 16-month-old KO mice (H) as compared to WT littermates (G). Scale bars: 500 µm. **(I-K)** Purkinje-cell loss in aged KO (J) but not WT (I) mice. Quantification of Purkinje cells (K) on hematoxylin-eosin stained cerebellum sections indicates a severe loss of Purkinje cells in aged KO mice (n=3; Student's t-test: *** indicates $p<0.001$). Scale bars: 40 µm.

Axon degeneration in *Spg11* knockout mice spinal cord

The thickness of the spinal cord of aged mice was reduced (data not shown). As one of the features of HSPs, histological analysis of semi-thin lumbar spinal cord sections

revealed that the number of large diameter axon fibers within the corticospinal tract of knockout mice were siginificantly reduced at 8 and 16 months of age, whereas, this difference was not detected between genotypes at 2 months of age (Fig. 11A-C). Swollen axons were already observed in lumbar regions of mutant mice spinal cord before overt loss of cortical motoneurons (Fig. 11D).

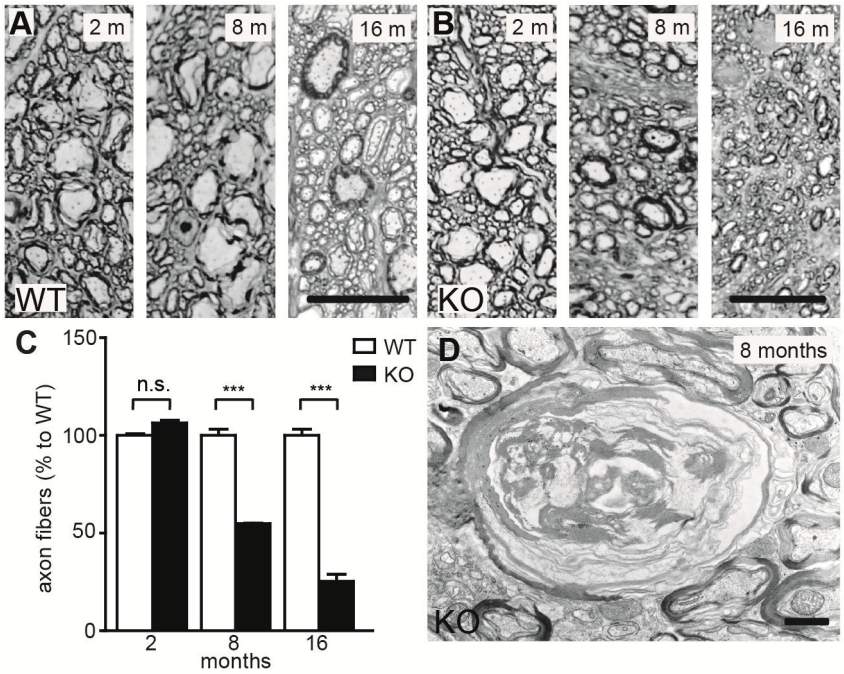

Figure 11. Spinal cord abnormalities in Spatacsin knockout mice
(A-C) Semithin sections of the lumbar corticospinal tract show a loss of large diameter axons in 8- and 16-month-old KO mice (n=3; Student's t-test: *** indicates $p<0.001$). Scale bars: 20µm. **(D)** Transmission electron microscopy of a degenerating axon in an 8-month-old KO mouse. Scale bar: 1 µm.

Neuron loss is preceded by the accumulation of autoflourescent material

In degenerating neurons we observed an intraneuronal accumulation of autofluorescent material (emission wavelength 460-630 nm) (Fig. 12A-D). This material was already present in knockout tissue at early time points (2 months) (Fig. 12B) and the amount of it drastically increased over time (Fig. 12D). In WT, autofluorescent material was only found in 16 months old mice and (Fig. 12C) appeared as small puncta like stuctures, whereas it was completely absent at 2 months of age (Fig. 12A). In KO, autofluorescent material also accumulated in neurons of other brain regions like hippocampus and spinal cord as well (Fig. 13B,F,J,N).

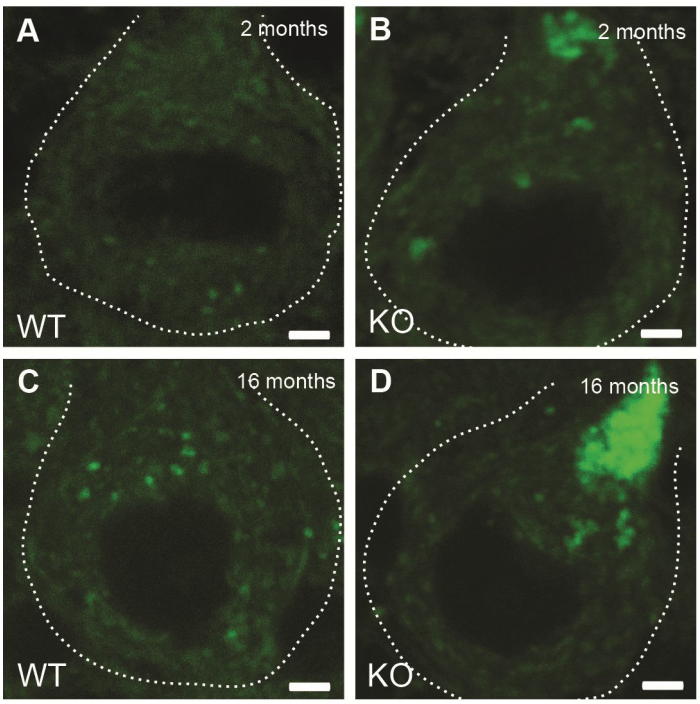

Figure 12. Accumulation of autofluorescent material in Purkinje cells of Spatacsin knockout mice
(A,C) In Purkinje cells of control mice no autofluorescent deposits were noted at 2 months of age (A), while some small (C) autofluorescent (AF) particles were found in 16 month old control mice. **(B,D)** Autofluorescent structures (AF) in KO Purkinje cells were already obvious at 2 months of age (B) and their amount dramatically increased over time (D). Purkinje cell somata are marked by a dashed line. Age and size at sampling: 16 months. AF: autofluorescence; Scale bars: 2.5 µm.

GFAP-positive astrocytes are abundant in brain regions with neuron loss

To monitor whether astrocytes respond to the observed neuron loss in knockout central nervous system, we stained tissue sections for the glial fibrillary acidic protein (GFAP). Increased expression of GFAP was restricted to CNS regions affected by neuron loss, namely the motorcortex, layers V and VI, and the cerebellum (Fig. 13A-D). GFAP immunreactivity was not changed in the hippocampus and the spinal cord , though neurons in these brain regions also accumulated autofluorescent material (Fig. 13I-P).

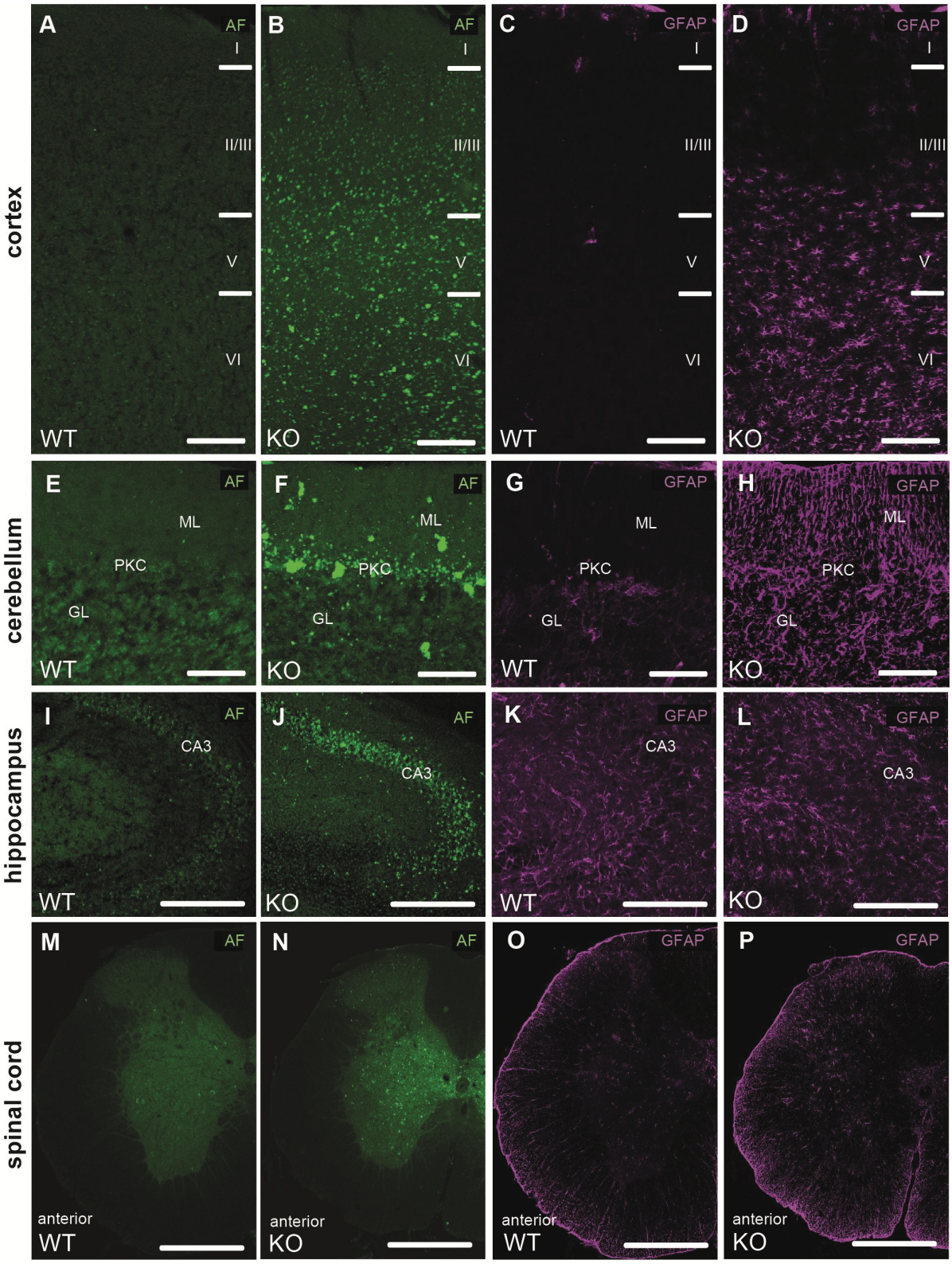

Figure 13. Autofluorescence and GFAP immunoreactivity in different regions of the central nervous system

(A-D) At 16 months of age we observed an accumulation of autofluorescent material in cortical neurons of Spatacsin KO mice (B). The neuron loss was paralleled by an activation of astrocytes in Spatacsin KO mice as evident from glial fibrillary acidic protein (GFAP) stainings (D). Cortical layers are labeled (I–VI). **(E-H)** Autofluorescent material also accumulated in the cerebellum of Spatacsin KO mice (F) and was paralleled by activation of

astrocytes (H). GL: granular cell layer, PKC: Purkinje cell layer, ML: molecular layer. Scale bars: 200 µm. **(I-P)** Neurons in the hippocampus (I-L) and the spinal cord (M-P) accumulate autofluorescent material, yet no activation of astroglia was observed in these regions. Scale bars: 150 µm (A-H) and 250 µm (I-P). CA3: Cornu ammonis 3. AF: autofluorescence.

Ultrastructural analysis reveals the accumulation of lipofuscin-like material in knockout Purkinje cells

Ultrastructural analysis of Purkinje cells revealed single membrane-bound vesicles filled with heterogeneous material including organelle-like structures at different stages of degradation in Spatacsin KO but not in WT mice (Fig. 14A-B´). In KO samples we further observed electron-dense deposits of irregular shape reminiscent of lipofuscin interspersed between abnormal autolysosomes (Fig. 14B´ arrow), while only some typical lipofuscin particles were found in controls of the same age (Fig. 14A´ arrowhead).

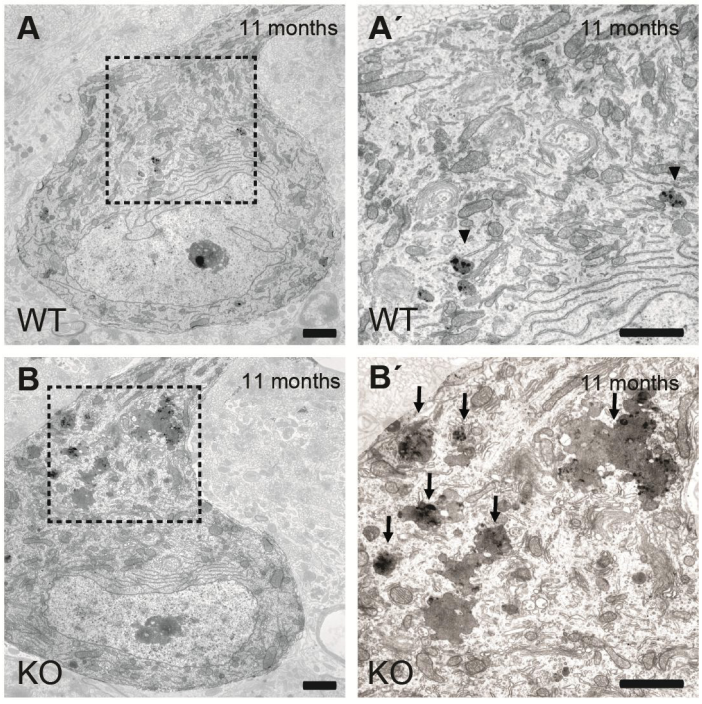

Figure 14. Lipofuscin-like material accumulates in Spatacsin knockout mice
(A-B´) Ultrastructural analysis of KO Purkinje cells reveals clusters of vesicular structures filled with autophagic material (arrows) and irregularly shaped electron-dense lipofuscin-like deposits (B´, arrow), while only some lipofuscin particles are found in WT (A´, arrowheads). Scale bars: 2 µm.

Degenerating neurons accumulate autophagy related material *in vivo*

To characterize the subcellular localization/origin of intraneuronal autofluorescent material in more detail, we stained brain sections of 11-month-old mice with different

subcellular marker proteins. Emission spectra of autofluorescent deposits and markers were separated by spectral analysis (Dickinson et al., 2001; Zimmermann et al., 2003). The periphery of the clustered autofluorescent material in Purkinje cells of KO mice was positive for the lysosomal marker Lamp1 (Fig. 15B-B´´). As the autofluorescent contents of these vesicular structures stained for p62 (Fig. 16B-B´´), a receptor for cargo destined to be degraded by autophagy, and LC3 (Fig. 17B-B´´), a membrane protein involved in autophagosome formation, these stuctures are most likely related to autolysosomes. Wild-type autofluorescent particles, on the contrary, barely colocalize with any of these markers (Fig. 15A-A´´; Fig. 16A-A´´; Fig. 17A-A´´). As a negative control, Giantin a marker for Golgi-apparatus was used, which did not colocalize with the deposits (data not shown). Taken together, knockout mice autoflourescent deposits likely represent abnormal autolysosomes.

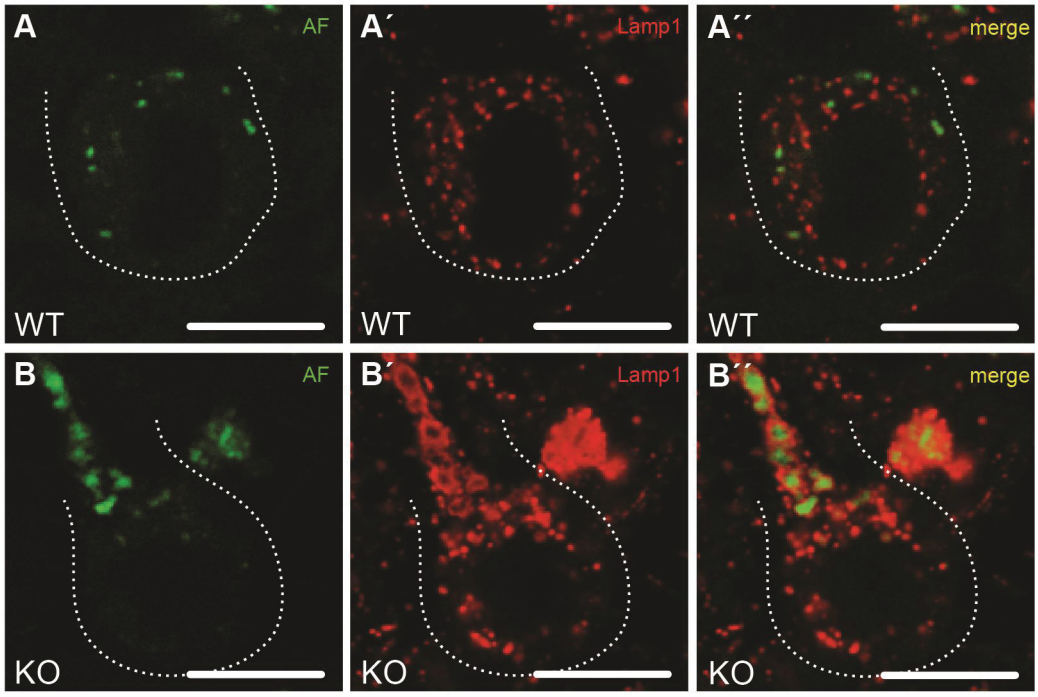

Figure 15. Autoflourescent deposits are surrounded by Lamp1 positive membranes in Spatacsin knockout mice
(A-B´´) While the small autofluorescent particles (AF) in WT Purkinje cells (A´´) are rarely associated with the lysosomal membrane protein Lamp1, autofluorescent structures in KO Purkinje cells stain for Lamp1 at their periphery (B´´). Age at sampling: 16 months. Lamp1: lysosomal marker; AF: autofluorescence; Scale bars: 2.5 µm.

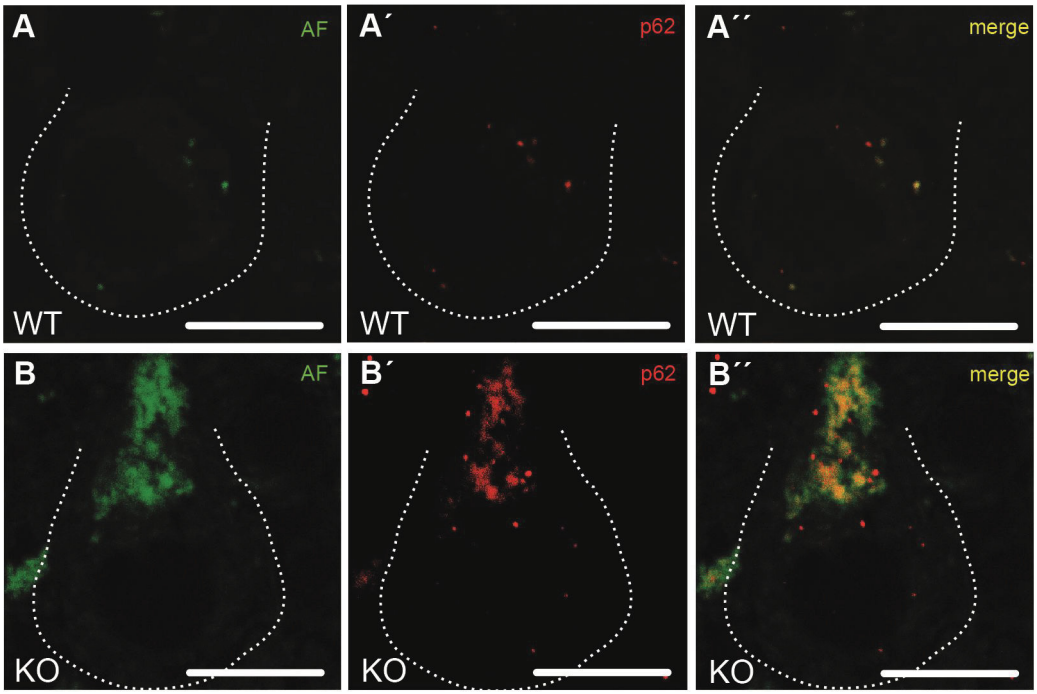

Figure 16. Autoflourescent structures colocalize with p62 in knockout mice
(A-B´´) The autofluorescent material in KO Purkinje cells colocalizes with p62 (B´´) whereas in WT these structures rarely associate with this marker (A´´). Purkinje cell somata are marked by a dashed line. Age at sampling: 16 months. AF: autofluorescence; Scale bars: 2.5 µm.

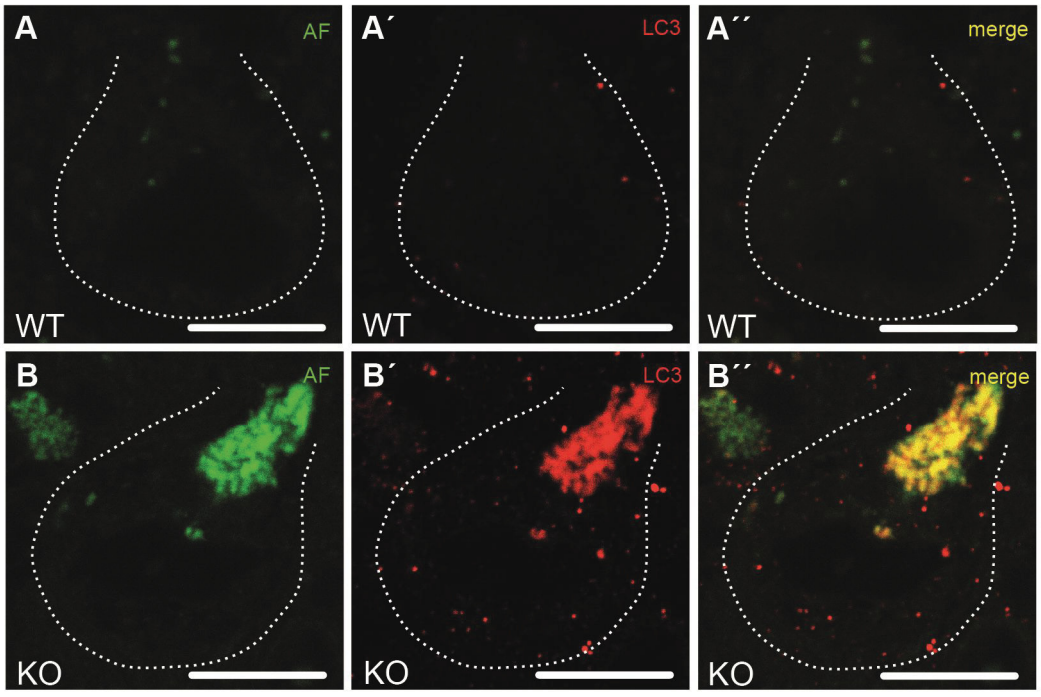

Figure 17. Autoflourescent material is positive for LC3 in knockout mice
(A-B´´) In KO Purkinje cells autofluorescent accumulations colocalize with LC3 (B´´).This was not observed in WT cells (A´´). Purkinje cell somata are marked by a dashed line. Age at sampling: 16 months. AF: autofluorescence; Scale bars: 2.5 µm.

Distinct features of lysosomal function are unaltered in knockout mice

To study what might be the underlying reason for the accumulation of undegraded material in autolysosomes we first investigated lysosomal function. We assessed the lysosomal processing of the lysosomal protease cathepsin D. Excluding a gross defect, the ratio between the mature and the precursor form of cathepsin D remained unchanged in KO brain lysates (Fig. 18A). Additionally, lysosomal pH as an important determinant for the activity of lysosomal proteases did not differ between genotypes in MEFs (Fig. 18B). Moreover the Lamp1 levels in KO brain lysates were not increased (Fig. 18C), a finding which was confirmed for KO MEF lysates as well (Fig. 18C).

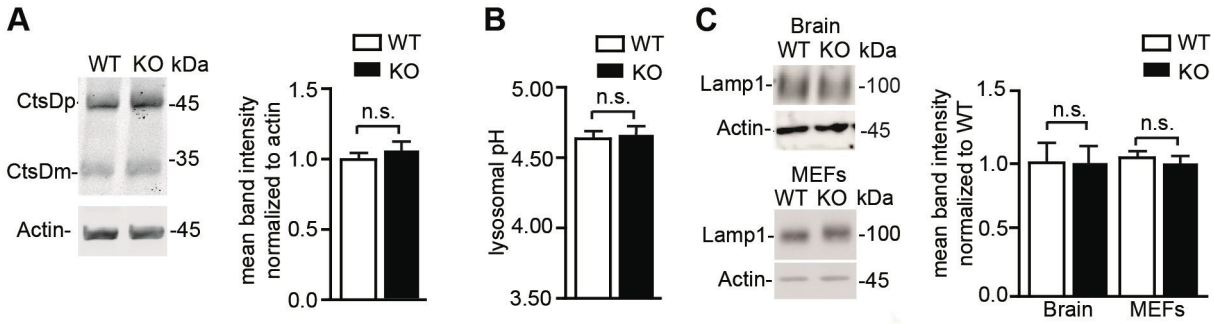

Figure 18. No obvious lysosomal defect upon Spatacsin disruption
(A) Lysosomal processing of the lysosomal protease Cathepsin D (CtsD) is not impaired in Spatacsin KO mice (CtsDp: precursor; CtsDm: mature). Mean+/- SEM of n=3 independent experiments; Student's T-test: not significant (n.s.). **(B)** The intralysosomal pH is not changed in KO MEFs. Mean+/-SEM of n=3 experiments with more than 1,000 lysosomes. Student's T-test: not significant (n.s.). **(C)** Overall Lamp1 levels are not changed in MEFs or brain lysates isolated from Spatacsin KO mice. Mean+/-SEM of n=3 independent experiments; Student's T-test: not significant (n.s.).

Autophagy is affected in knockout mice

Ultrastructural analysis revealed that apart from the accumulation of lipofuscin-like material (Fig. 19A arrowhead), also clusters of vesicular structures filled with autophagic material (Fig. 19A arrows) were found in samples of KO mice. We therefore assessed whether autophagy is affected upon *Spg11* disruption. By immunoblotting we analysed the amount of Beclin-1, a key protein for autophagosome formation (Mizushima et al., 2011), which was unaltered (Fig. 19B-B´), indicating that initial steps of autophagy may not be blocked upon disruption of Spatacsin. Interestingly, we found that the levels of the autophagic cargo marker p62 (Lamark et al. 2009) were strongly elevated in the Triton X-100 insoluble fractions of KO brain lysates as compared to WT (Fig. 19B-B´), which rather point to a defect in

later stages of autophagic clearance. Furthermore, elevated basal levels of LC3-II (the lipidated form of LC3 which is incorporated into the autophagic membrane) further increased upon treatment with bafilomycin A1 in fibroblasts (MEFs) isolated from Spatacsin KO embryos (Fig. 19C-C´).

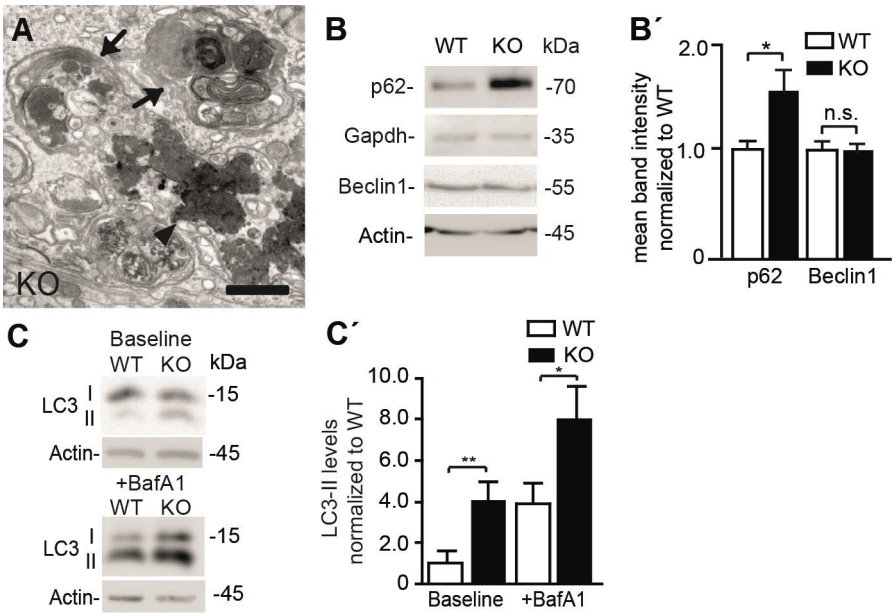

Figure 19. LC3-II and p62 levels are increased in knockout mice
(A) Accumulation of lipofuscin-like material (arrowhead) and autophagic material (arrows) in 11 month old KO tissue. Scale bars: 2 µm. **(B-B´)** p62, a marker for cargo destined to be degraded by autophagy, is increased in Triton X-100 insoluble brain fractions of 16-month-old Spatacsin KO mice, while Beclin 1, a key protein for the formation of autophagosomes, is not changed. Mean +/- SEM; n=3 each; Student's T-test: not significant (n.s.); * indicates $p<0.05$. **(C-C´)** LC3-II levels are increased in KO MEFs and further increase after treatment with bafilomycin A1. Quantification of LC3-II levels normalized to actin in MEFs. Mean +/- SEM of 4 independent experiments; Student´s T-test: ** indicates $p<0.005$ and * $p<0.05$.

Autophagic lysosomal reformation (ALR) is impaired in knockout mice

To assess whether the accumulation of autolysosomes in Spatacsin KO mice is accompanied by a depletion of lysosomes, as is expected if ALR is impaired, we investigated the process ALR in MEFs. We found that the number of autolysosomes were increased (Fig. 20A), at the same time the number of lysosomes were decreased in KO MEFs (Fig. 20B). Moreover, lysosomes were depleted upon induction of autophagy by starvation for 6 h in both WT and KO MEFs. Only WT lysosome numbers recovered to baseline after 14 h of ongoing starvation while they remained diminished in KO MEFs (Fig. 20C-J).

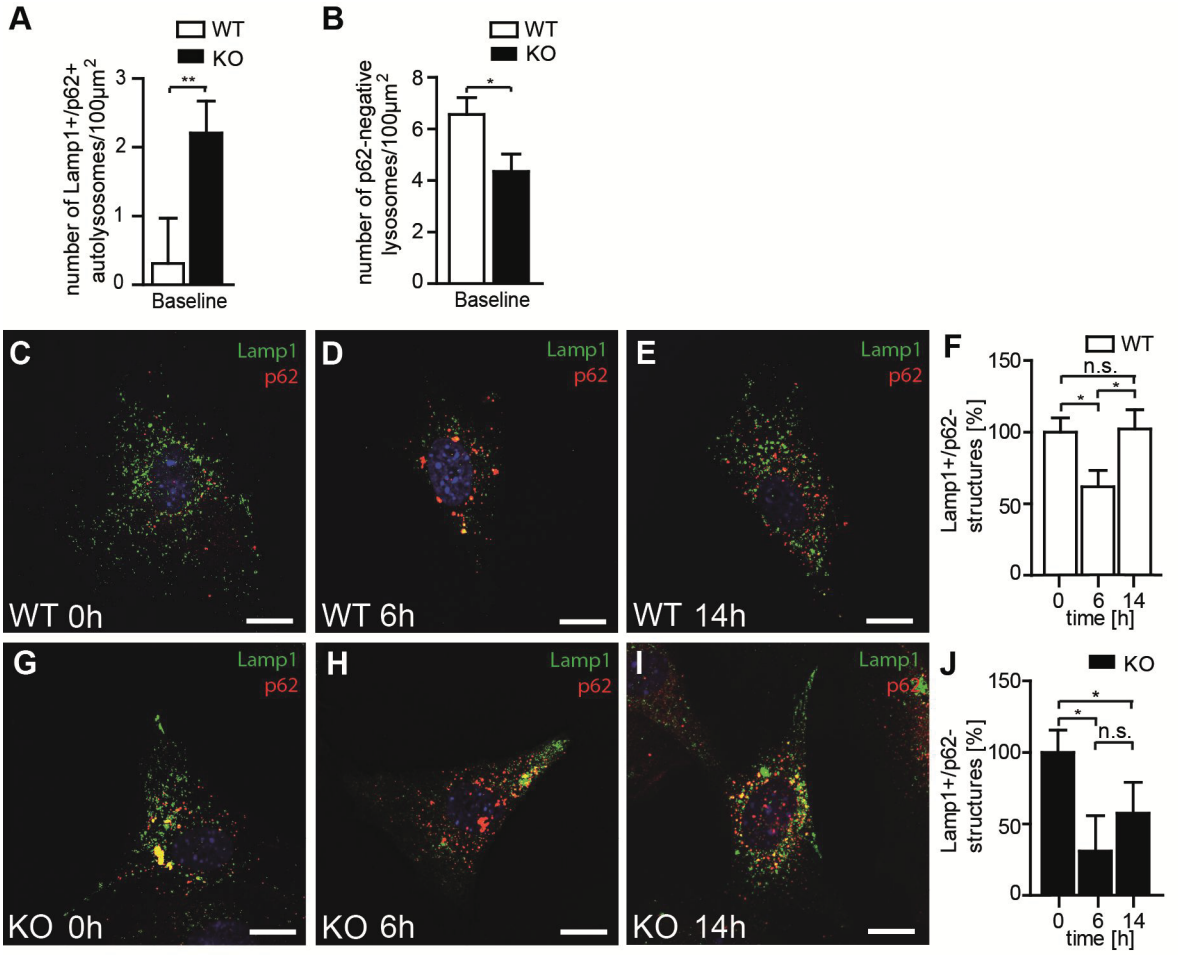

Figure 20. Decreased regeneration of free lysosomes in knockout mice
(A) Autolysosomes, vesicles that stain for both Lamp1 and p62, are increased in KO MEFs compared to WT. Student's t-test: ** indicates $p<0.01$. **(B)** Lysosomes defined as vesicles positive for Lamp1 but negative for p62 are decreased under baseline conditions in Spatacsin KO MEFs. Student's t-test: * indicates $p<0.05$ **(C-J)** Upon 6 h of starvation lysosomes were depleted in both WT and KO MEFs. After 14 h lysosome numbers recovered to baseline levels only in WT. Mean±SEM of n=10; one-way-ANOVA: * indicates $p<0.05$. Scale bars: 10 µm.

We also investigated whether ALR was also affected *in vivo* at sites where neuron loss was observed (e.g.:cerebellum). Lamp1-positive and p62-negative vesicles in Purkinje cell somata of 2 and 11-month-old mice (Fig. 21A-B´´) were quantified revealing that the number of lysosomes was decreased in Purkinje cells of Spatacsin KO mice (Fig. 21C) both at 2 and 11 months of age.

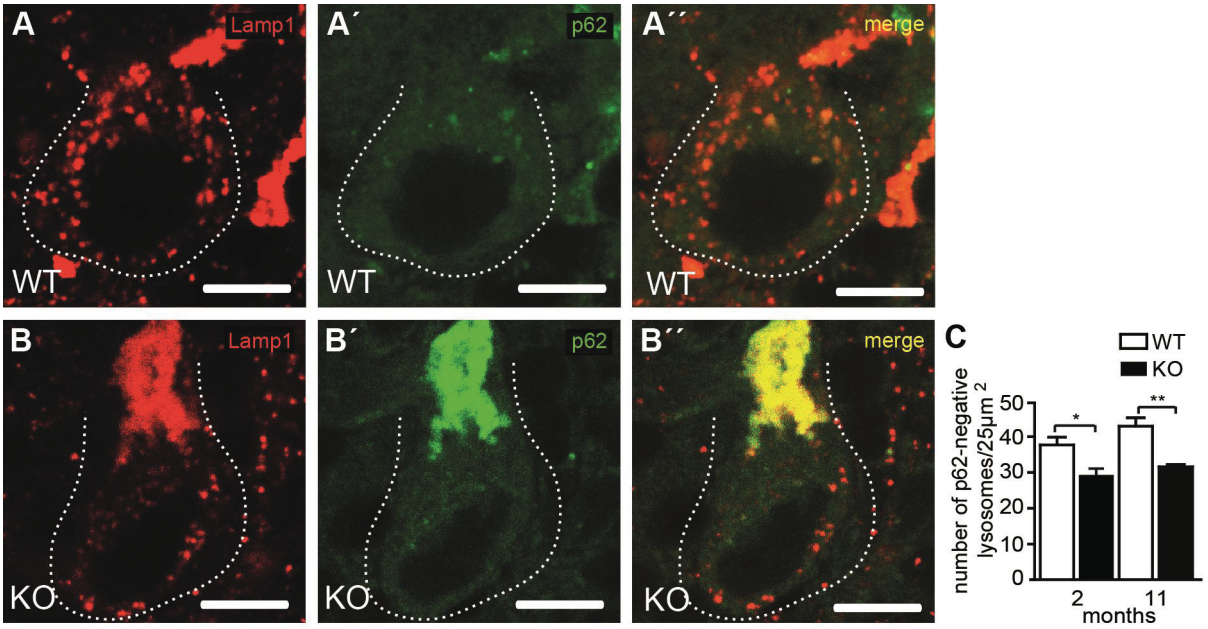

Figure 21. Depletion of free lysosomes in Spatacsin knockout mice

(A-C) Free Lysosomes, defined as vesicles positive for Lamp1 but negative for p62 in 11 months old tissue (A-B´´) are decreased in Purkinje cells of both 2 and 11-month-old Spatacsin KO mice as compared to WT (C). Mean +/- SEM; n=22 cells each; two-way-ANOVA: * indicates $p<0.05$, ** indicates $p<0.005$. Purkinje cell somata are marked by a dashed line. Scale bars: 2.5 µm.

Discussion

Verification of *Spg11* knockout mice

HSP type SPG11 is the most common autosomal recessive, complicated form of HSPs. To date, the mutational spectrum of SPG11 includes numerous missense, nonsense, splice site mutations as well as small indels, small and gross deletions or insertions. The effect of these mutations on the protein level is supposed to lead to a truncated or non-functional protein (Stevanin et al., 2007; Hehr et al., 2007). Consequently, the homozygous *Spg11* knockout is the relevant *in vivo* model to study SPG11. To generate Spatacsin KO mice we used a gene trap clone. During the trapping process the gene trap vector -containing the gene trap cassette- randomly inserts into a genomic locus of ES cells and thus disturbs the transcription of the trapped gene resulting in a truncated mRNA which is translated into a non-functional, truncated protein (Schnutgen et al., 2005). Our gene trap cassette – consisting of a 5' splice acceptor site (SA), a promoterless reporter gene (βgeo) and 3' polyadenylation site (pA) (Fig. 7A´) - is integrated into the first intron of *Spg11* (Fig. 7A). The presence of the cassette in the mutant animals was confirmed by genotyping PCR identifying a 256 bp WT and a 167 bp KO band as expected. (Fig. 7B) (Fig. 6). The transcribed mRNA is predicted to be truncated, consistently, Northern Blot analysis using a probe targeting a part of exon 30 of *Spg11* detected a 7.6 kb transcript in wild-type tissue samples which was absent from knockout samples (Fig. 7C). The predicted *Spg11* mRNA transcript encodes a cytoplasmic fusion protein of the 82 N-terminal amino acids of Spatacsin with βgeo under the control of the endogenous *Spg11* promoter (Fig. 7A'''). In order to confirm the loss of Spatacsin in mice, we generated a monoclonal antibody directed against an epitope within the α-solenoid domain of Spatacsin (Fig. 7A'' arrowhead). Our antibody detected Spatacsin at the expected size of roughly 270 kDa in control samples, and this signal was not present in knockout tissue lysates (Fig. 7D) confirming the specificity of the antibody.

Thus, we validated our constituve *Spg11* mouse model by demonstrating (1) the presence of the trap cassette on DNA level, (2) the absence of mRNA transcript and (3) subsequently the protein product. Consequently, the homozygous gene trap mice represent the Spatacsin KO model. Moreover, we (4) present the first specific and verified anti-Spatacsin antibody as well.

Tissue expression of *Spg11*/Spatacsin

Expression analysis by *in situ* hybridization of the rat *Spg11* mRNA in rat adult brain revealed strong *Spg11* expression in the pineal gland, the edges of the lateral ventricles, the granular layer of the cerebellum and the hippocampus (Stevanin et al., 2008). To note, no *Spg11* mRNA expression was detected in newborn rats (Stevanin et al., 2008). Interestingly, the expression of *spg11* mRNA during zebrafish development by whole mount *in situ* hybridization depicted ubiquitous *spg11* expression with stong expression levels in the brain (Southgate et al., 2010). Later, the Stevanin group showed by an antibody (validated by peptide blocking) detecting the endogenous SPATACSIN/Spatacsin in human and rat adult tissues, that its expression was predominantly found at layer V of the motor cortex, spinal cord, hippocampus, cerebellum, dentate nucleus and pons (Murmu et al., 2011). Moreover, using the same antibody ubiquitous Spatacsin expression was found in all tissues of rat embryos (Murmu et al., 2011). In the nervous sytem SPATACSIN/Spatacsin was shown to be specific to neurons (Murmu et al., 2011; Perez-Branguli et al., 2014).

The presence of the genetrap cassette expressed under the endogenous promoter of the *Spg11* gene provided us a straightforward tool to investigate *Spg11* expression.

Our data obtained from Lac-Z stainings on tissue sections of heterozygous trapped mice revealed a neuronal expression pattern of *Spg11.* Partially in agreement with the previous studies, signals detected by Lac-Z staining were particularly strong in cortical neurons (Fig. 8A), spinal cord neurons (Fig. 8B), and cerebellar Purkinje cells (Fig. 8C) and were absent in tissue sections of wild-type mice.

Simultaneously, we also tried to detect the endogenous Spatacsin by our novel and specific antibody by immunofluorescence but we were not able to detect a specific signal on tissue sections.

To summarize, our results strengthen the point that *Spg11* seems to be specific to neurons, however, the tissue expression of *Spg11*/Spatacsin has not yet been completely clarified due to the lack of specific antibodies detecting endogenous Spatacsin in immunofluorescence. This issue, therefore, needs further investigation.

Spg11 knockout mice develop complicated HSP

SPG11 patients usually show several additional symptoms ranging from thin corpus callosum, to cognitive decline, peripheral neuropathy and cerebellar ataxia (Stevanin et al., 2007; Hanein et al., 2008; Schüle et al., 2011).

Both non-vertebrate and vertebrate animal models have already been used to model HSP *in vivo* in order to elucidate the function of a certain HSP gene product. Genetic manipulation of the fruit fly *Drosophila melanogaster* have been used to clarify the physiological roles of SPG4, SPG6, SPG3A, SPG12 and SPG10 (Sherwood et al., 2004; Orso et al., 2005; Wang et al., 2007; Lee et al., 2009; O'Sullivan et al., 2012; Füger et al, 2012). To assess the motor defects of mutant fruit flies either climbing assay (Orso et al., 2005; Lee et al., 2008; O'Sullivan et al., 2012; Füger et al, 2012) or locomotor assay (Füger et al, 2012) was applied.

The vertebrate *Danio rerio* is an established tool to investigate gene function *in vivo*. Its advantages include high fecundity, easy visualization due to the transparency of its embryos and short generation time (Xi et al., 2011). To date, several zebrafish HSP models exist, which show reduced motility and curly tail (Wood et al., 2006; Lin et al., 2008; Fassier et al., 2010; Clemen et al., 2010; Butler et al., 2010; Campbell et al., 2013). Accordingly, morpholino knock-down of Spatacsin or Spastizin in the zebrafish resulted in motor impairment with the typical curly tail phenotype and abnormal branching of spinal cord motor neurons at the neuromuscular junction (Martin et al., 2012).

The above mentioned models have limitations regarding their relevance for the HSP movement phenotype. Hence, evolutionary closer relatives, such as rodents are more disease relevant *in vivo* model systems.

Untill present numerous HSP genes have so far been knocked out in mice using different methods for prooving the motor impairment i.e.: rotarod (Ferreirinha et al., 2004; Pirozzi et al., 2006), catwalk (Kasher et al., 2009), beam walking and measuring the number of falls and slips (Soderblom et al., 2010; Khundadze et al., 2013) or quantifying the foot stepping angle (Beetz et al., 2013; Khundadze et al., 2013).

The current work aimed not only to address whether mice lacking functional Spatacsin develop a motor phenotype but also to give a comprehensive comparison to the already published HSP mouse models.

Accordingly, motor coordination was addressed by an accelerating rotating rod and showed that aged *Spg11* knockout mice fell off the rod significantly earlier as compared to wild-type controls (Fig. 9D). In order to quantify the gait abnormality we also analysed the foot base angle (FBA) of the hindpaws at toe-off position (Fig. 9A-B) (Irintchev et al., 2005) during beam walking. At 12 months of age, knockout mice had siginificantly smaller FBA as compared to wild-type littermates. Moreover, the value of knockout FBA gradually decreased over time (Fig. 9C). To investigate ataxia we quantified the number of slips and falls during mice traversing a 2 cm thin beam. Old knockout mice fell off the beam significantly more frequently than wild-type littermates (Fig. 9E).

Another aspect of the human HSP phenotype is the length-dependent degeneration of the corticospinal tract axon fibers (Blackstone et al., 2011; Harding et al., 1983). Analysis of semi-thin lumbar spinal cord sections confirmed the loss of large diameter axon fibers within the corticospinal tract already at 8 months of age whereas spinal cord of young mice was intact (Fig. 11A-C) a finding which has also been described for other mouse models of HSP (Ferreirinha et al., 2004; Tarrade et al., 2006; Beetz et al. 2013, Khundadze et al., 2013).
Besides, in lumbar regions of 8-month-old mutant mice swollen axon fibers were observed (Fig. 11D) similarly to *Zfyve26* knockout mice (Khundadze et al., 2013).
Furthermore, in conrast to pure HSP mouse models (Ferreirinha et al., 2004; Tarrade et al., 2006; Beetz et al., 2013) and in concert with the previous results of our group (Khundadze et al., 2013), *Spg11* knockout mice loose the large projection motoneurons in motocortex layers V/VI, indicating that the cellular pathology is not restricted to motoneuron axons, but also affects the somata, as obvious from the quantification of NeuN-positive neurons in the motocortex. (Fig. 10D-F).
On the contrary, neuron numbers in layers I-III, where most of the commissural neurons reside (Greig et al., 2013), remained unchanged (Fig. 10F). Consistently, the size of the corpus callosum was unaltered in aged knockout mice (Fig. 10G-H). This discrepancy to the human phenotype may be due to the fact that in mice the size of corpus callosum strongly depends on the respective mouse strain (Boettger et al., 2003; Wahlsten et al., 1982).

Importantly, neuron loss was not only restricted to the deep layers of the motor cortex but was also detected in the cerebellar cortex affecting Purkinje cells (Fig. 10I-K) consistent with ataxia and the cerebellar atrophy observed in these animals. Furthermore, as typical for central nervous system injury (Pekny et al., 2005), GFAP positive astrocytes became abundant at the sites of the neuronal loss in aged knockout mice. (Fig. 11A-D).

To sum up, *Spg11* knockout mice developed complicated HSP i.e.: progressive motor impairement and gait disorder paralleled with ataxia, weight loss (Fig. 9F) and an abnormal kyphotic posture. Histopathological analyses of the central nervous system confirmed brain atrophy, which is especially severe in the cerebellum (Fig. 10A-B) concomitantly, revealed the loss of cortical motoneurons and cerebellar Purkinje cells, furthermore the degeneration of axon fibers in the corticospinal tract. In agreement with previous studies (Fink et al., 2006) which stated that SPG11 is presumably a neurodegenerative disease, *Spg11* knockout mice show no structural or motor deficit till 12 months of age.

Cellular pathology related to Spatacsin dysfunction

Prior to the onset of motor deficit and neuron loss, similarly to *Zfyve26* knockout mice (Khundadze et al., 2013), intraneuronal accumulation of autofluorescent material was observed in *Spg11* knockout mice (Fig. 12B). The amount of this material drastically increased over time (Fig. 12D). Whereas in WT, this material was only very limited in aged mice (Fig. 12C) and was absent at young age (Fig. 12A). Ultrastructural analysis revealed that these structures were similar to lipofuscin particles found in aged WT, however, in knockout tissue these were found more frequently, often clustered and surrounded by membrane (Fig. 14A-B´).

Interestingly, autofluorescent material in knockout tissue also accumulated in brain regions like hippocampus as well as spinal cord (Fig. 13B,N) where no activation of astrocyes was observed (Fig. 13L,P). This is in sharp contrast with results obtained from brain regions with obvious neuron loss (Fig. 13A-D). This discrepancy might be due the vulnerability of large neurons in the motorcortex and cerebellum, while neurons in other brain regions may tolerate these autofluorescent lipofuscin like deposits.

Lipofuscin is a lipopigment consisting of approximately 70% proteins and 30% lipids and less than 2 % metals (Brunk et al., 2002). Due to its broad excitation and emission spectra it has autofluorescent property (Schnell et al., 1999). This substance either accumulates in postmitotic cells as a result of senescene (Brunk et al., 2002) or due to certain genetic conditions, such as neuronal ceroid lipofuscinosis (Seehafer et al., 2006; Weimer et al., 2002) or retinal dystrophy (Radu et al., 2008). It is considered to be a non-degradable material related to lysosomes (Terman et al., 2004). Indeed, our results showed that autofluorescent accumulation in knockout neurons were labeled by the lysosomal marker Lamp1 (Fig. 15A-A´´).

Lysosomes are digestive components of the autophagic pathway (Kiel et al., 2010). During autophagy cargo -such as aggregate prone proteins- is sequestered by a double membrane vesicle called autophagosome which fuses with lysosomes in order to promote degradation (Eskelinen et al., 2009). Recently, it has been shown that Spastizin interacts with Beclin-1 (Vantaggiato et al., 2013) a subunit of the phosphatidylinositol 3-kinase class III (PI3K-III) complex, which is located on early endosomes (Simonsen et al., 1998). Besides it is a key regulator of the initial steps of autophagy. As revealed from patient derived fibroblasts, when Spastizin was mutated, then this interaction was disturbed which did not interrupt with the formation of Beclin-1 complex and therefore led to the accumulation of autophagosomes (Vantaggiato et al., 2013).

Suggesting that autophagy may be possibly also altered in *Spg11* knockout mice, autofluorescent deposits indeed stained for p62 (Fig. 16A-A´´), an autophagosomal cargo receptor indicating that these autofluorescent accumulations rather represent abnormal autolysosomes instead of lysosomes. Moreover, ultrastructural analysis revealed membrane-bound vesicles filled with heterogeneous material including organelle-like structures (Fig. 17A arrows) suggesting that it may be autophagic material, consistent with the immunofluorescence results in Purkinje neurons (Fig. 16A-A´´). These results may suggest that the membranous structures reported in sural nerve biopsies (Hehr et al., 2007) and iPSC-derived neurons from SPG11 patients (Perez-Branguli et al., 2014) may represent abnormal autolysosomes.

In agreement with our findings in Purkinje cells, in baseline conditions the number of autolysosomes, defined as vesicles labeled for both Lamp1 and p62 was increased

in KO MEFs (Fig. 20A), while at the same time the number of lysosomes was decreased in KO MEFs (Fig. 20B).

Moreover, certain lysosomal functions in *Spg11* knockout mice remained intact as the processing of brain Cathepsin D (Fig. 18A) and lysosomal pH in MEFs (Fig. 18B) were unchanged as compared to wild-type samples. Moreover, Lamp1 levels in both KO brain and MEF lysates were not elevated (Fig. 18C). Since, we investigated only a part of the numerous lysosomal functions therefore it cannot be excluded that some of these may also be altered.

Beclin-1 (responsible for autophagosome formation) levels remained unchanged (Fig. 19B-B´), pointing out that the initial steps of autophagy may not be affected when functional Spatacsin is not present. As expected, p62 and LC3II levels were increased (Fig. 19B-C´), suggesting that the defect may be at later stages of the autophagic pathway.

The (1) accumulation of autolysosomal material together with (2) unaltered lysosomal function and (3) unaffected autophagosome formation, in contrast, (4) elevated levels of autophagic cargo receptor (p62) and its interacting partner (LC3) suggest that the fusion of lysosomes with autophagosomes still occurs while autophagic clearance is impaired. This points to the direction that later stages of the autopagic pathway may be affected upon Spatacsin disruption.

Non-functional Spatacsin and ALR

A recent report showed *in vitro* on HeLa cells that Spatacsin and Spastizin were essential for the regeneration of lysosomes from autolysosomes, a process known as autophagic lysosome reformation (ALR) (Chang et al., 2014), which has so far only been observed *in vitro* (Shen et al., 2014). According to this model impaired ALR leads to exhaustion of lysosomes available for fusion of autophagosomes and accumulation of autolysosomes. As expected, our results corroborate these findings both *in vitro* and *in vivo*, i.e.: the number of autolysosomes were increased (Fig. 20A), simultaneously the number of lysosomes were decreased in KO MEFs (Fig. 20B). Furthermore, upon starvation induced autophagy for 6 h lysosomes were depleted in both WT and KO MEFs. Interestingly, only WT lysosome numbers recovered to the baseline condition after 14 h of ongoing starvation while KO MEFs lysosome numbers did not recover (Fig. 20C-J). Moreover, quantification of Lamp1-positive and

p62-negative vesicles *in vivo* at the sites of neurodegeneration i.e.: Purkinje cell somata of 2 and 11-month-old mice (Fig. 21A-B´´) revealed that the number of lysosomes was decreased in Purkinje cells of Spatacsin KO mice (Fig. 21C) both at 2 and 11 month of age.

Upon Spatacsin disruption ALR is impaired hence the number of lysosomes does not recover to the baseline condition in knockout MEFS, furthermore the number of lysosomes is depleted in knockout Purkinje cells *in vivo*. This is in agreement with our observation that old knockout mice have drastic accumulation of autolysosomal materal which may be the result of the long-term ALR defect.

Spatacsin as the interacting partner of the AP5 complex

Spatacsin interacts with the recently identified adaptor complex AP-5 (Hirst et al., 2011). Initially, the members of this complex have been suggested to be crucial for DNA repair (Slabicki et al., 2010). Later, these were confirmed to be the subunits of the AP-5 complex which has been suggested to localize to late endosomes/lysosomes and to be involved in the sorting of cargo along the endo-lysosomal system (Fig. 4) (Hirst et al., 2013). Based on secondary structure predictions, it has been speculated that Spatacsin may form a scaffold coat around AP-5 in a clathrin-like manner, while Spastizin may serve to dock AP-5 to specific membranes (Hirst et al., 2013). Consequently, the siRNA knockdown of either protein results in the decrease of the other one. Similarly, our results depict that Spastizin is decreased in *Spg11* knockout mice whereas the ß-subunit of the AP-5 complex (Hirst et al., 2011) is unaltered upon *Spg11* disruption (Fig. 7E-G). The zeta subunit of AP-5 (AP-5ζ) is mutated in SPG48 (Slabicki et al., 2010) and these patients have very similiar clinical phenotype to that of SPG11 and SPG15 (Pensato et al., 2014), therefore it is possible that *Spg11* disruption has no effect on the amount of the ß-subunit of the AP-5 complex.

We, therefore, provide the first evidence that ALR may be of relevance *in vivo*. Concerning the function of the Spatacsin protein, it cannot be excluded that Spatacsin has an AP5 dependent and independent function as well.

In case of the latter one, it seems that disruption of Spatacsin leads to the accumulation of autolysosomes and to the depletion of lysosomes available for fusion

with autophagosomes both *in vitro* and *in vivo* which may lead in the long term to the death of particularly sensitve neurons.

On the other hand, it is also plausible that lack of Spatacsin leads to the disintegrity of the AP5 complex hence either a cargo may be missorted or a cargo destinied to be delivered to the lysosome may be mistargeted which may also lead to lysosomal dysfunction and therefore the decreased turnover of autolysosomes.

Outlook

Since it is possible that the accumulation of deposits may result from the disintegrity of the AP5 complex, therefore upon Spatacsin disruption maybe the cargo of AP-5 accumulates as deposits in knockout mice. Thus it would be interesting to investigate the deposits by mass-spectrometry. Lipofilic deposits can be isolated by gradient centrifugation and can be further analyzed (Ottis et al., 2012). Interestingly, in a form of neuronal ceroid lipofuscinosis the accumulation of the c-subunit of ATP-synthase is found (Schultz et al., 2011).

Another way would be to use *stable isotpe labeling with amino acids in cell culture* (SILAC) assay (Ong et al., 2002) on knockout and wild-type cells and perform mass-spectrometry analyzes afterwords.

These approaches would provide quantitative analyses and may therefore lead to a better clarification of the disease.

As protein aggregation is a common phenomenon in neurodegenerative disease. In numerous neurodegenerative disorders the different protein degradation pathways play a coordinated role in removing the aggregates (Ciechanover et al., 2015). Therefore it may be interesting to assess if the ubiquitin-proteasome system as well as the chaperone mediated autophagy are affected when Spatacsin is lost.

Literature

Abada A, Elazar Z, et al. (2014) Getting ready for building: signaling and autophagosome biogenesis. EMBO Rep. 2014 Aug;15(8):839-52.

Amritraj A, Wang Y, Revett TJ, Vergote D, Westaway D, Kar S, et al. (2013) Role of cathepsin D in U18666A-induced neuronal cell death: potential implication in Niemann-Pick type C disease pathogenesis. J Biol Chem. 2013 Feb 1;288(5):3136-52.

Anheim M, Lagier-Tourenne C, Stevanin G, Fleury M, Durr A, Namer IJ, Denora P, Brice A, Mandel JL, Koenig M, Tranchant C, et al. (2009) SPG11 spastic paraplegia. A new cause of juvenile parkinsonism. J Neurol. 2009 Jan;256(1):104-8.

Bauer P, Leshinsky-Silver E, Blumkin L, Schlipf N, Schroder C (2012) Mutation in the AP4B1 gene cause hereditary spastic paraplegia type 47 (SPG47). Neurogenetics 13: 73-76.

Beetz C, Koch N, Khundadze M, Zimmer G, Nietzsche S, Hertel N, Huebner AK, Mumtaz R, Schweizer M, Dirren E, Karle KN, Irintchev A, Alvarez V, Redies C, Westermann M, Kurth I, Deufel T, Kessels MM, Qualmann B, Hübner CA, et al. (2013) A spastic paraplegia mouse model reveals REEP1-dependent ER shaping. J Clin Invest. 2013 Oct;123(10):4273-82.

Blackstone C, O'Kane CJ, Reid E, et al. (2011) Hereditary spastic paraplegias: membrane traffic and the motor pathway. Nat Rev Neurosci. 2011;1:31-42.

Blackstone C (2012) Cellular pathways of hereditary spastic paraplegia. Annu Rev Neurosci. 2012;35:25-47.

Boettger T, Rust MB, Maier H, Seidenbecher T, Schweizer M, et al. (2003) Loss of K-Cl cotransporter KCC3 causes deafness, neurodegeneration and reduced seizure threshold. EMBO J 22: 5422-5434.

Braschinsky M, Luus SM, Gross-Paju K, Haldre S, et al. (2008) The Prevalence of Hereditary Spastic Paraplegia and the Occurrence of SPG4 Mutations in Estonia. Neuroepidemiology 32: 89-93.

Brunk UT, Terman A, et al. (2002) Lipofuscin: mechanisms of age-related accumulation and influence on cell function. Free Radic Biol Med 33: 611-619.

Butler R, Wood JD, Landers JA, Cunliffe VT, et al. (2010) Genetic and chemical modulation of spastin-dependent axon outgrowth in zebrafish embryos indicates a role for impaired microtubule dynamics in hereditary spastic paraplegia. Dis Model Mech. 2010 Nov-Dec;3(11-12):743-51.

Campbell PD, Marlow FL, et al. (2013) Temporal and tissue specific gene expression patterns of the zebrafish kinesin-1 heavy chain family, kif5s, during development. Gene Expr Patterns. 2013 Oct;13(7):271-9.

Carlsson SR, Simonsen A, et al. (2015) Membrane dynamics in autophagosome biogenesis. J Cell Sci. 2015 Jan 15;128(2):193-205.

Carpenter MB. (1991) Core Text of Neuroanatomy. Baltimore, MD: Wilkins & Wilkins. 4th ed.

Cerminara NL, Lang EJ, Sillitoe RV, Apps R, et al. (2015) Redefining the cerebellar cortex as an assembly of non-uniform Purkinje cell microcircuits. Nat Rev Neurosci. 2015 Feb;16(2):79-93.

Chang J, Lee S, Blackstone C, et al. (2014) Spastic paraplegia proteins spastizin and spatacsin mediate autophagic lysosome reformation. J Clin Invest 124: 5249-5262.

Clemen CS, Tangavelou K, Strucksberg KH, Just S, Gaertner L, Regus-Leidig H, Stumpf M, Reimann J, Coras R, Morgan RO, Fernandez MP, Hofmann A, Müller S, Schoser B, Hanisch FG, Rottbauer W, Blümcke I, von Hörsten S, Eichinger L, Schröder R, et al. (2010) Strumpellin is a novel valosin-containing protein binding partner linking hereditary spastic paraplegia to protein aggregation diseases. Brain. 2010 Oct;133(10):2920-41.

DeLuca GC, Ebers GC, Esiri MM, et al. (2004) The extent of axonal loss in the long tracts in hereditary spastic paraplegia. Neuropathol. Appl. Neurobiol. 30(6):576–84.

Depienne C, Stevanin G, Brice A, Durr A, et al. (2007) Hereditary spastic paraplegias: an update. Curr Opin Neurol 20: 674-680.

Deretic V (2010) A Master Conductor for Aggregate Clearance by Autophagy. Dev Cell. 2010 May 18; 18(5): 694–696.

Dickinson ME, Bearman G, Tille S, Lansford R, Fraser SE, et al. (2001) Multi-spectral imaging and linear unmixing add a whole new dimension to laser scanning fluorescence microscopy. Biotechniques 31: 1272, 1274–1276, 1278.

Eskelinen EL, Saftig P, et al. (2009) Autophagy: a lysosomal degradation pathway with a central role in health and disease. Biochim Biophys Acta. 2009 Apr;1793(4):664-73.

Faber I, Servelhere KR, Martinez AR, D'Abreu A, Lopes-Cendes I, França-Jr MC, et al. (2014) Clinical features and management of hereditary spastic paraplegia. Arq Neuropsiquiatr. 2014 Mar;72(3):219-26.

Fassier C, Hutt JA, Scholpp S, Lumsden A, Giros B, Nothias F, Schneider-Maunoury S, Houart C, Hazan J, et al. (2010) Zebrafish atlastin controls motility and spinal motor axon architecture via inhibition of the BMP pathway. Nat Neurosci. 2010 Nov;13(11):1380-7.

Ferreirinha F, Quattrini A, Pirozzi M, Valsecchi V, Dina G, et al. (2004) Axonal degeneration in paraplegin-deficient mice is associated with abnormal mitochondria and impairment of axonal transport. J Clin Invest 113: 231-242.

Filimonenko M, Isakson P, Finley KD, Anderson M, Jeong H, Melia TJ, Bartlett BJ, Myers KM, Birkeland HC, Lamark T, Krainc D, Brech A, Stenmark H, Simonsen A, Yamamoto A, et al. (2010) The selective macroautophagic degradation of aggregated proteins requires the PI3P-binding protein Alfy. Mol Cell. 2010 Apr 23;38(2):265-79.

Fink JK (2006) Hereditary spastic paraplegia. Curr Neurol Neurosci Rep 6: 65-76.

Finsterer J, Loscher W, Quasthoff S, Wanschitz J, Auer-Grumbach M, et al. (2012) Hereditary spastic paraplegias with autosomal dominant, recessive, X-linked, or maternal trait of inheritance. J Neurol Sci 318: 1-18.

Füger P, Sreekumar V, Schüle R, Kern JV, Stanchev DT, Schneider CD, Karle KN, Daub KJ, Siegert VK, Flötenmeyer M, Schwarz H, Schöls L, Rasse TM, et al. (2012) Spastic paraplegia mutation N256S in the neuronal microtubule motor KIF5A disrupts axonal transport in a Drosophila HSP model. PLoS Genet. 2012;8(11):e1003066.

Greig LC, Woodworth MB, Galazo MJ, Padmanabhan H, Macklis JD, et al. (2013) Molecular logic of neocortical projection neuron specification, development and diversity. Nat Rev Neurosci 14: 755-769.

Hanein S, Martin E, Boukhris A, Byrne P, Goizet C, et al. (2008) Identification of the SPG15 gene, encoding spastizin, as a frequent cause of complicated autosomal recessive spastic paraplegia, including Kjellin syndrome. Am J Hum Genet 82: 992-1002.

Harding AE (1983) Classification of the hereditary ataxias and paraplegias. Lancet 1: 1151-1155.

Hehr U, Bauer P, Winner B, Schule R, Olmez A, Koehler W, Uyanik G, Engel A, Lenz D, Seibel A, Hehr A, Ploetz S, Gamez J, Rolfs A, Weis J, Ringer TM, Bonin M, Schuierer G, Marienhagen J, Bogdahn U, Weber BH, Topaloglu H, Schols L, Riess O, Winkler J, et al. (2007) Long-term course and mutational spectrum of spatacsin-linked spastic paraplegia. Ann Neurol. 2007 Dec;62(6):656-65.

Hirst J, Barlow LD, Francisco GC, Sahlender DA, Seaman MN, et al. (2011) The fifth adaptor protein complex. PLoS Biol 9: e1001170.

Hirst J, Irving C, Borner GH, et al. (2013) Adaptor Protein Complexes AP-4 and AP-5: New Players in Endosomal Trafficking and Progressive Spastic Paraplegia. Traffic 14: 153-164.

Ichimura Y, Komatsu M, et al. (2010) Selective degradation of p62 by autophagy. Semin Immunopathol. 2010 Dec;32(4):431-6.

Irintchev A, Simova O, Eberhardt KA, Morellini F, Schachner M, et al. (2005) Impacts of lesion severity and tyrosine kinase receptor B deficiency on functional outcome of

femoral nerve injury assessed by a novel single-frame motion analysis in mice. Eur J Neurosci 22: 802-808.

Jackson LP, Kelly BT, McCoy AJ, Gaffry T, James LC, Collins BM, Höning S, Evans PR, Owen DJ, et al. (2010) A Large-Scale Conformational Change Couples Membrane Recruitment to Cargo Binding in the AP2 Clathrin Adaptor Complex. Cell. 2010 June 25; 141(7): 1220–1229.

Jones ML, Murden SL, Brooks C, Maloney V, Manning RA, Gilmour KC, Bharadwaj V, de la Fuente J, Chakravorty S, Mumford AD, et al. (2013) Disruption of AP3B1 by a chromosome 5 inversion: a new disease mechanism in Hermansky-Pudlak syndrome type 2. BMC Med Genet. 2013 Apr 4;14:42.

Kankaanpaa P, Paavolainen L, Tiitta S, Karjalainen M, Paivarinne J, et al. (2012) BioImageXD: an open, general-purpose and high-throughput image-processing platform. Nat Methods 9: 683-689.

Kasher PR, De Vos KJ, Wharton SB, Manser C, Bennett EJ, Bingley M, Wood JD, Milner R, McDermott CJ, Miller CC, Shaw PJ, Grierson AJ, et al. (2009) Direct evidence for axonal transport defects in a novel mouse model of mutant spastin-induced hereditary spastic paraplegia (HSP) and human HSP patients. J Neurochem. 2009 Jul;110(1):34-44.

Khundadze M, Kollmann K, Koch N, Biskup C, Nietzsche S, Zimmer G, Hennings JC, Huebner AK, Symmank J, Jahic A, Ilina EI, Karle K, Schöls L, Kessels M, Braulke T, Qualmann B, Kurth I, Beetz C, Hübner CA, et al. (2013) A hereditary spastic paraplegia mouse model supports a role of ZFYVE26/SPASTIZIN for the endolysosomal system. PLoS Genet. 2013;9(12):e1003988.

Kiel JA. (2010) Autophagy in unicellular eukaryotes. Philos Trans R Soc Lond B Biol Sci. 365(1541):819-30.

Klionsky DJ (2011) Autophagy: from phenomenology to molecular understanding in less than a decade. Nature Reviews Molecular Cell Biology 8, 931-937.

Kollmann K, Uusi-Rauva K, Scifo E, Tyynelä J, Jalanko A, Braulke T. (2013) Cell biology and function of neuronal ceroid lipofuscinosis-related proteins. Biochim Biophys Acta. S0925-4439(13)00033-1.

Kong XF, Bousfiha A, Rouissi A, Itan Y, Abhyankar A, Bryant V, Okada S, Ailal F, Bustamante J, Casanova JL, Hirst J, Boisson-Dupuis S, et al. (2013) A novel homozygous p.R1105X mutation of the AP4E1 gene in twins with hereditary spastic paraplegia and mycobacterial disease. PLoS One. 2013;8(3):e58286.

Lamark T, Kirkin V, Dikic I, Johansen T, et al. NBR1 and p62 as cargo receptors for selective autophagy of ubiquitinated targets. Cell Cycle. 2009 Jul 1;8(13):1986-90.

Lee M, Paik SK, Lee MJ, Kim YJ, Kim S, Nahm M, Oh SJ, Kim HM, Yim J, Lee CJ, Bae YC, Lee S, et al. (2009) Drosophila Atlastin regulates the stability of muscle

microtubules and is required for synapse development. Dev Biol. 2009 Jun 15;330(2):250-62.

Lin P, Li J, Liu Q, Mao F, Li J, Qiu R, Hu H, Song Y, Yang Y, Gao G, Yan C, Yang W, Shao C,Gong Y. (2008). A missense mutation in SLC33A1, which encodes the acetyl-CoA transporter, causes autosomal-dominant spastic paraplegia (SPG42). Am J Hum Genet 83: 752-759.

Lübke T, Lobel P, Sleat DE, et al. (2009) Proteomics of the lysosome. Biochim Biophys Acta. 2009 Apr;1793(4):625-35.

Martin E, Yanicostas C, Rastetter A, Naini SM, Maouedj A, et al. (2012) Spatacsin and spastizin act in the same pathway required for proper spinal motor neuron axon outgrowth in zebrafish. Neurobiol Dis 48: 299-308.

Mizushima N, Komatsu M, et al. (2011) Autophagy: renovation of cells and tissues. Cell 147: 728-741.

Moreno-De-Luca A, Helmers SL, Mao H, Burns TG, Melton AM, Schmidt KR, Fernhoff PM, Ledbetter DH, Martin CL, et al. (2011) Adaptor protein complex-4 (AP-4) deficiency causes a novel autosomal recessive cerebral palsy syndrome with microcephaly and intellectual disability. J Med Genet. 2011 Feb;48(2):141-4.

Murmu RP, Martin E, Rastetter A, Esteves T, Muriel MP, et al. (2011) Cellular distribution and subcellular localization of spatacsin and spastizin, two proteins involved in hereditary spastic paraplegia. Mol Cell Neurosci 47: 191-202.

Najmabadi H, Hu H, Garshasbi M, Zemojtel T, Abedini SS, Chen W, Hosseini M, Behjati F, Haas S, Jamali P, Zecha A, Mohseni M, Püttmann L, Vahid LN, Jensen C, et al. (2011) Deep sequencing reveals 50 novel genes for recessive cognitive disorders. Nature 2011;478:57–63.

Novarino G, Fenstermaker AG, Zaki MS, Hofree M, Silhavy JL, et al. (2014) Exome sequencing links corticospinal motor neuron disease to common neurodegenerative disorders. Science 343: 506-511.

Ong SE, Blagoev B, Kratchmarova I, Kristensen DB, Steen H, Pandey A, Mann M, et al. (2002) Stable isotope labeling by amino acids in cell culture, SILAC, as a simple and accurate approach to expression proteomics. Mol Cell Proteomics. 2002 May;1(5):376-86.

Orlacchio A, Babalini C, Borreca A, Patrono C, Massa R, Basaran S, Munhoz RP, Rogaeva EA, St George-Hyslop PH, Bernardi G, Kawarai T, et al. (2010) SPATACSIN mutations cause autosomal recessive juvenile amyotrophic lateral sclerosis. Brain. 2010 Feb;133(Pt 2):591-8.

Orlén H, Melberg A, Raininko R, Kumlien E, Entesarian M, Söderberg P, Påhlman M, Darin N, Kyllerman M, Holmberg E, Engler H, Eriksson U, Dahl N, et al. (2009) SPG11 mutations cause Kjellin syndrome, a hereditary spastic paraplegia with thin

corpus callosum and central retinal degeneration. Am J Med Genet B Neuropsychiatr Genet. 2009 Oct 5;150B(7):984-92.

Orso G, Martinuzzi A, Rossetto MG, Sartori E, Feany M,Daga A, et al. (2005). Disease-related phenotypes in a Drosophila model of hereditary spastic paraplegia are ameliorated by treatment with vinblastine. J Clin Invest 115: 3026-3034.

O'Sullivan NC, Jahn TR, Reid E, O'Kane CJ, et al. (2012) Reticulon-like-1, the Drosophila orthologue of the hereditary spastic paraplegia gene reticulon 2, is required for organization of endoplasmic reticulum and of distal motor axons. Hum Mol Genet. 2012 Aug 1;21(15):3356-65.

Ottis P, Koppe K, Onisko B, Dynin I, Arzberger T, Kretzschmar H, Requena JR, Silva CJ, Huston JP, Korth C, et al., (2012) Human and rat brain lipofuscin proteome. Proteomics. 2012 Aug;12(15-16):2445-54.

Peden AA, Oorschot V, Hesser BA, Austin CD, Scheller RH, Klumperman J, et al. (2004) Localization of the AP-3 adaptor complex defines a novel endosomal exit site for lysosomal membrane proteins. J Cell Biol. 2004 Mar 29;164(7):1065-76.

Pekny M, Nilsson M, et al. (2005) Astrocyte activation and reactive gliosis. Glia 50: 427-434.

Pensato V, Castellotti B, Gellera C, Pareyson D, Ciano C, et al. (2014) Overlapping phenotypes in complex spastic paraplegias SPG11, SPG15, SPG35 and SPG48. Brain 137: 1907-1920.

Perez-Branguli F, Mishra HK, Prots I, Havlicek S, Kohl Z, et al. (2014) Dysfunction of spatacsin leads to axonal pathology in SPG11-linked hereditary spastic paraplegia. Hum Mol Genet 23: 4859-4874.

Pirozzi M, Quattrini A, Andolfi G, Dina G, Malaguti MC, Auricchio A,Rugarli EI, et al. (2006) Intramuscular viral delivery of paraplegin rescues peripheral axonopathy in a model of hereditary spastic paraplegia. J Clin Invest 116: 202-208.

Poirier S, Mayer G, Murphy SR, Garver WS, Chang TY, Schu P, Seidah NG, et al. (2013) The cytosolic adaptor AP-1A is essential for the trafficking and function of Niemann-Pick type C proteins.Traffic. 2013 Apr; 14(4): 458–469.

Radu RA, Yuan Q, Hu J, Peng JH, Lloyd M, Nusinowitz S, Bok D, Travis GH, et al. (2008) Accelerated accumulation of lipofuscin pigments in the RPE of a mouse model for ABCA4-mediated retinal dystrophies following Vitamin A supplementation. Invest Ophthalmol Vis Sci. 2008 Sep;49(9):3821-9.

Reid E (1999) The hereditary spastic paraplegias. J Neurol 246: 995-1003.

Repnik U, Stoka V, Turk V, Turk B, et al. (2012) Lysosomes and lysosomal cathepsins in cell death. Biochim. Biophys. Acta 1824, 22–33.

Robinson MS, Sahlender DA, Foster SD,et al. (2010) Rapid inactivation of proteins by rapamycin-induced rerouting to mitochondria. Dev Cell. 2010 Feb 16;18(2):324-31.

Rong Y, Liu M, Ma L, Du W, Zhang H, Tian Y, Cao Z, Li Y, Ren H, Zhang C, Li L, Chen S, Xi J, Yu L, et al. (2012) Clathrin and phosphatidylinositol-4,5-bisphosphate regulate autophagic lysosome reformation. Nat Cell Biol. 2012 Sep;14(9):924-34.

Sauter S, Miterski B, Klimpe S, Bönsch D, Schöls L, Visbeck A, Papke T, Hopf HC, Engel W, Deufel T, Epplen JT, Neesen J, et al. (2002) Mutation analysis of the spastin gene (SPG4) in patients in Germany with autosomal dominant hereditary spastic paraplegia. Hum Mutat. 2002 Aug;20(2):127-32.

Seehafer SS, Pearce DA (2006) You say lipofuscin, we say ceroid: Defining autofluorescent storage material. Neurobiol Aging 27(4):576-88.

Sherwood NT, Sun Q, Xue M, Zhang B, Zinn K, et al. (2004) Drosophila spastin regulates synaptic microtubule networks and is required for normal motor function. PLoS Biol. 2004 Dec;2(12):e429.

Schmahmann JD (2004) Disorders of the cerebellum: ataxia, dysmetria of thought, and the cerebellar cognitive affective syndrome. J Neuropsychiatry Clin Neurosci. 2004 Summer;16(3):367-78.

Schnell SA, Staines WA, Wessendorf MW, et al. (1999) Reduction of lipofuscin-like autofluorescence in fluorescently labeled tissue. J Histochem Cytochem. 1999 Jun;47(6):719-30.

Schnutgen, F., S. De-Zolt, et al. (2005) "Genomewide production of multipurpose alleles for the functional analysis of the mouse genome." Proc Natl Acad Sci U S A 102(20): 7221-6.

Schultz ML, Tecedor L, Chang M, Davidson BL, et al. (2011) Clarifying lysosomal storage diseases. Trends Neurosci. 2011 Aug;34(8):401-10.

Schüle R, Schols L (2011) Genetics of hereditary spastic paraplegias. Semin Neurol 31: 484-493.

Shen HM, Mizushima N, et al. (2014) At the end of the autophagic road: an emerging understanding of lysosomal functions in autophagy. Trends Biochem Sci 39: 61-71.

Simonsen A, Lippé R, Christoforidis S, Gaullier JM, Brech A, Callaghan J, Toh BH, Murphy C, Zerial M, Stenmark H. (1998) EEA1 links PI(3)K function to Rab5 regulation of endosome fusion. Nature 394(6692):494-8.

Simmen T, Höning S, Icking A, Tikkanen R, Hunziker W, et al. (2002) AP-4 binds basolateral signals and participates in basolateral sorting in epithelial MDCK cells. Nat Cell Biol. 2002 Feb;4(2):154-9.

Slabicki M, Theis M, Krastev DB, Samsonov S, Mundwiller E, et al. (2010) A genomescale DNA repair RNAi screen identifies SPG48 as a novel gene associated with hereditary spastic paraplegia. PLoS Biol 8: e1000408.

Soderblom C, Stadler J, Jupille H, Blackstone C, Shupliakov O, Hanna MC, et al. (2010) Targeted disruption of the Mast syndrome gene SPG21 in mice impairs hind limb function and alters axon branching in cultured cortical neurons. Neurogenetics. 2010 Oct;11(4):369-78.

Southgate L, Dafou D, Hoyle J, Li N, Kinning E, Critchley P, Németh AH, Talbot K, Bindu PS, Sinha S, Taly AB, Raghavendra S, Müller F, Maher ER, Trembath RC, et al. (2010) Novel SPG11 mutations in Asian kindreds and disruption of spatacsin function in the zebrafish. Neurogenetics. 2010 Oct;11(4):379-89.

Stevanin G, Santorelli FM, Azzedine H, Coutinho P, Chomilier J, et al. (2007) Mutations in SPG11, encoding spatacsin, are a major cause of spastic paraplegia with thin corpus callosum. Nat Genet 39: 366-372.

Stevanin G, Ruberg M, Brice A (2008) Recent advances in the genetics of spastic paraplegias. Curr Neurol Neurosci Rep. May;8(3):198-210.

Stolz A., Ernst A., Dikic I, et al. (2014) Cargo recognition and trafficking in selective autophagy. Nat. Cell Biol. 16 495–501 10.1038/ncb2979.

Tarrade A, Fassier C, Courageot S, Charvin D, Vitte J, et al. (2006) A mutation of spastin is responsible for swellings and impairment of transport in a region of axon characterized by changes in microtubule composition. Hum Mol Genet 15: 3544-3558.

Terman A, Brunk UT, et al. (2004) Lipofuscin. Int J Biochem Cell Biol 36: 1400-1404.

Vantaggiato C, Crimella C, Airoldi G, Polishchuk R, Bonato S, et al. (2013) Defective autophagy in spastizin mutated patients with hereditary spastic paraparesis type 15. Brain 136: 3119-3139.

Verkerk AJ, Schot R, Dumee B, Schellekens K, Swagemakers S, Bertoli-Avella AM, Lequin MH, Dudink J, Govaert P, van Zwol AL, Hirst J, Wessels MW, Catsman-Berrevoets C, Verheijen FW, de Graaff E, de Coo IF, Kros JM, Willemsen R, Willems PJ, van der Spek PJ, Mancini GM, et al. (2009) Mutation in the AP4M1 gene provides a model for neuroaxonal injury in cerebral palsy. Am J Hum Genet. 2009 Jul;85(1):40-52.

Wahlsten D (1982) Deficiency of corpus callosum varies with strain and supplier of the mice. Brain Res 239: 329-347.

Wang X, Shaw WR, Tsang HT, Reid E,O'Kane CJ, et al. (2007) Drosophila spichthyin inhibits BMP signaling and regulates synaptic growth and axonal microtubules. Nat Neurosci 10: 177-185.

Weimer JM, Kriscenski-Perry E, Elshatory Y, Pearce DA, et al. (2002) The neuronal ceroid lipofuscinoses. Mutations in different proteins result in similar disease. Neuromol Med 1: 111–124.

Weinert S, Jabs S, Supanchart C, Schweizer M, Gimber N, et al. (2010) Lysosomal pathology and osteopetrosis upon loss of H+-driven lysosomal Cl- accumulation. Science 328: 1401–1403.

Wood JD, Landers JA, Bingley M, McDermott CJ, Thomas-McArthur V, Gleadall LJ, Shaw PJ,Cunliffe VT. (2006). The microtubule-severing protein Spastin is essential for axon outgrowth in the zebrafish embryo. Hum Mol Genet 15: 2763-2771.

Xi Y, Noble S, Ekker M, et al. (2011) Modeling Neurodegeneration in Zebrafish. Curr Neurol Neurosci Rep. 2011 June; 11(3): 274–282.

Zimmermann T, Rietdorf J, Pepperkok R, et al. (2003) Spectral imaging and its applications in live cell microscopy. FEBS Lett 546: 87–92.

Zuchner S. (2007) The genetics of hereditary spastic paraplegia and implications for drug therapy. Expert Opin Pharmacother 8: 1433-1439.

Appendix

Acknowledgments

First and foremost I would like to express my deepest appreciation to my supervisor, Prof. Christian Hübner. He has always been a great support since the day I joined his lab. He taught me how to tackle scientific problems, provided academic guidance, a very motivating and creative research environment and gave me all the facilities to do research. Also, he encouraged me to collaborate with other scientists therefore opened doors for me to get to know different interntaional researchers. Without his generous and persistent guidance this thesis and my topic would have not been successfull. He is a passionate and successful scientist who inspires me to pursue career in science.

Secondly, I would like to express my gratitude towards all members of the 'HSP research group- Jena'. I am very happy that Prof Hübner gave me the opportunity to work together with a fantastic scientist, Dr. Christian Beetz. Throughout my PhD, Christian was always very encouraging and helped me with his suggestions. Importantly, he taught me how to think critically when analyzing and solving scientific issues which helped me to evolve as a scientist for which I am very thankful for him. I also wish to thank Dr. Mukhran Khundadze who is a talented young scientist. Mukhran shared his experience and great expertise with me and working with him was not only very productive but also cheering up because he is apart from being a smart researcher also has a very good sense of humor. I would like to thank my lovely collegues, Annette Büschel, Heike Kiesewetter and Kerstin Stein who helped me to learn laboratory techniques. Their protective and caring nature made feel like I had three friends beside me every day when I went to work. Without their consistent help I also would not be able to speak German as I do now. I am very happy that I got to know all of them.

Thirdly, I would like to thank all members of the Hübner Lab for accepting me and letting me integrate to the group from the very first moment. I am very lucky to have been able to have you as my collegues. I especially would like to thank Dr. Jean-Christopher Hennings for helping me to learn the Northern Blot technique. Christopher, you are a great person, a talented, smart and hard-working scientist,

and one of the main ‘motor’ of our lab who next to directing his own projects always ready to help everyone in the lab.

Also, I sincerely thank all the scientists outside my lab who collaborated with me on my PhD project. It has been a great pleasure to get to know you and to work with all of you. I appreciate all of your efforts and contribution to make my project successfull.

I am genuinely grateful to Prof Regine Heller who I can thank for the fact that I am working in Jena. She interviewd me on a very stormy afternoon in 2010 June and later accepted me to the first Molecular Medicine Summer School held in Jena. I feel very lucky that I got to know you Regine, you are a lovely person and a great support for each and every student including me as well.

Lastly, I would like to thank my beloved family: my mother, my father, my grandmother and my uncle and his family for being always there for me. Without your love, support and encouragement I would not be at the stage where I am today.

Ehrenwörtliche Erklärung

Hiermit erkläre ich, dass mir die Promotionsordnung der Medizinischen Fakultät der Friedrich-Schiller-Universität bekannt ist, ich die Dissertation selbst angefertigt habe und alle von mir benutzten Hilfsmittel, persönlichen Mitteilungen und Quellen in meiner Arbeit angegeben sind, mich folgende Personen bei der Auswahl und Auswertung des Materials sowie bei der Herstellung des Manuskripts unterstützt haben: Prof. Dr. Christian Hübner, Dr. Christian Beetz, Dr. Mukhran Khundadze, PD Dr. Ingo Kurth, Dr. Sandor Nietzsche und Prof. Dr. Regine Heller, die Hilfe eines Promotionsberaters nicht in Anspruch genommen wurde und dass Dritte weder unmittelbar noch mittelbar geldwerte Leistungen von mir für Arbeiten erhalten haben, die im Zusammenhang mit dem Inhalt der vorgelegten Dissertation stehen, dass ich die Dissertation noch nicht als Prüfungsarbeit für eine staatliche oder andere wissenschaftliche Prüfung eingereicht habe und ass ich die gleiche, eine in wesentlichen Teilen ähnliche oder eine andere Abhandlung nicht bei einer anderen Hochschule als Dissertation eingereicht habe.

Jena, 28.07.2015. _____

Rita Eva Varga